STRESS OPTIMIZATION OF RHOMBIC TRANSPOSITION FLAPS USING THE FINITE ELEMENT METHOD

A Thesis Submitted to the College of

Graduate Studies and Research

In Partial Fulfillment of the Requirements

For the Degree of Master of Science

In the Department of Mechanical Engineering

University of Saskatchewan

Saskatoon

By

Amirhossein Rajabi

Permission to Use

In presenting this thesis in partial fulfilment of the requirements for a Postgraduate degree from the University of Saskatchewan, I agree that the Libraries of this University may make it freely available for inspection. I further agree that permission for copying of this thesis in any manner, in whole or in part, for scholarly purposes may be granted by the professor or professors who supervised my thesis work or, in their absence, by the Head of the Department or the Dean of the College in which my thesis work was done. It is understood that any copying or publication or use of this thesis or parts thereof for financial gain shall not be allowed without my written permission. It is also understood that due recognition shall be given to me and to the University of Saskatchewan in any scholarly use which may be made of any material in my thesis.

Requests for permission to copy or to make other use of material in this thesis in whole or part should be addressed to:

Head of the Department of Mechanical Engineering

57 Campus Drive, University of Saskatchewan

Saskatoon, Saskatchewan

Canada, S7N 5A9

Abstract

Use of local skin flaps is a common practice in plastic and reconstructive surgery for complex wound closure. As a consequence of transposing these flaps, however, a stress field is created throughout the tissue. Previous work suggests a relationship between the stress field and a reduction in blood flow which can delay the process of wound healing, and may also cause many undesirable effects on tissue functionality.

The objective of this research was to design an optimized version of rhombic transposition flaps by minimization of maximum von Mises stress with constraints on maximum compressive stress and undeformed/deformed configurations. To accomplish this objective, a finite element (FE) model was developed within a commercially available FE analysis package (ANSYS®). It used an Ogden hyperelastic material model with reliable geometry/meshing to ensure convergent results. It also incorporated a novel approach to model sutures. To study material uncertainties of skin, four different sets of constants were used. By defining flap geometry using adjustable parameters, the process of wound closure was simulated for a large number of configurations to identify optimized configurations.

The results suggest a design that is comparable in design to Z-plasty and can be easily implemented. The proposed flap, which can be employed for 60° to 90° rhombic defects, reduced the maximum von Mises stress by 43% and 53% (on average) with respect to the flaps of Limberg (60° defect) and Dufourmentel (60° to 90° defects), respectively.

Acknowledgments

I wish to express my deepest gratitude and sincere thanks to my supervisor, Professor Allan Dolovich, for his valuable guidance, financial support, considerable encouragement, patience, and extremely amazing caring. He has been extremely supportive in all the stages of this study, from developing the research hypothesis to writing the thesis.

I would like to express my sincere appreciations to Professor James Johnston, my committee Chair, for his continuous encouragement, valuable guidance, and useful comments to enhance the quality of my research.

I also take this opportunity to express my sincere gratitude to Professor Chris Zhang, my committee member, for all his valuable guidance, especially at the beginning of my studies at the University of Saskatchewan.

I am also deeply grateful to all of my lovely friends for their unceasing encouragement and support. They have always been there for me.

Finally, I would like to express my very profound appreciation and gratitude to my beloved family, for their unconditional love, never-ending support, and continuous encouragement.

To my beloved parents, Ali and Maryam

Table of Contents

List of Tables

List of Figures

1. Introduction

1.1. Problem Statement

In plastic and reconstructive surgery, the majority of excised skin lesions can be directly closed by creating elliptical defects. As the size or complexity of a lesion increases, however, there is a stage when direct wound closure is not possible. In many such cases, a local flap is employed, whereby part of the tissue with an intact blood supply is lifted from a local site and pulled to fill a defect. To illustrate this surgical technique, three simple types of local flap are shown in Figure 1.1.

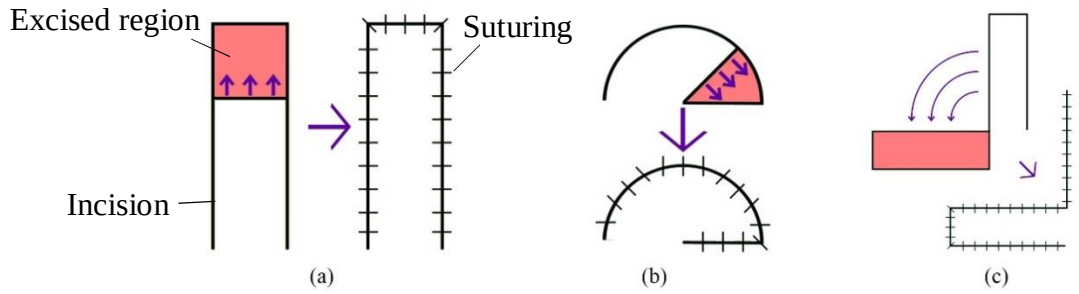

Figure 1.1 Three simple types of local flap: (a) advancement flap, (b) rotation flap, and (c) transposition flap.[1]

To create a simple advancement flap, as shown in Figure 1.1(a), the area of interest is cut out so that a square region is formed. Next, two more incisions are made along two parallel sides of the defect, and then the rectangular-shape tissue is detached from its beneath surface. Finally, the created flap is stretched over the defect to make it possible for suturing and completing the process

[1] Modified Taylornate, 2011. Available at: https://en.wikipedia.org/wiki/Flap_(surgery)

of wound closure. Similarly, Figure 1.1(b) and (c) show a simple rotation flap and a simple transposition flap, respectively. Basically, a transposition flap is a combination of an advancement flap and a rotation flap.

The flap of interest to be investigated in this research is the rhombic transposition flap (Figure 1.2(a)). To construct such a flap, first, the lesion is revised and excised so that a rhombic area ABCD, with an acute angle ϕ, is created. Then, the flap is constructed by creating two more incisions, first from D to E at an angle θ_1 measured from an imaginary line extending from the short diagonal BD, and then a second incision from E to F at an angle θ_2 with respect to ED. In general, all the sides of the defect and the added incisions have the same length. The whole process of transposition is illustrated in Figure 1.2.

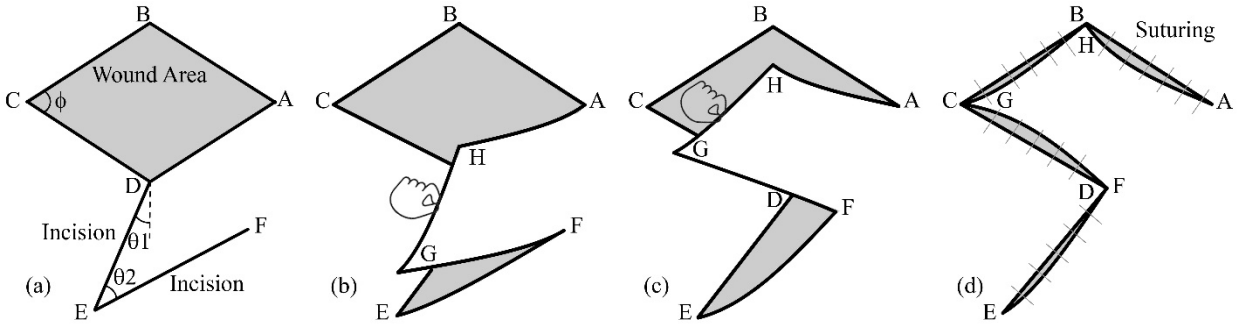

Figure 1.2 The rhombic transposition flap

The use of local flaps creates a stress field in the tissue, and this has been of indispensable importance in design problems. Others have referenced this stress field in terms of a "tension" which is created in the tissue and must be minimized (Borges, 1978; Danielson, 1978). Based on the reported correlation with blood flow, a reduction in this tension can reduce healing time, and also prevent many undesirable effects such as necrosis formation, dehiscence, granulation, and ischemia (Bucalo and Iriondo, 1995; Cacou and Muir, 1995; Danielson and Natarajan, 1975; Lister and Gibson, 1972). Preventing large compressive stresses can also be of great help as a means of

avoiding depressed areas in skin such as dog-ear formation (Limberg, 1966; Lister and Gibson, 1972).

In the design for rhombic flaps, there have been a number of variations with a special attention to stress considerations. Among them are the flaps of Limberg (Limberg, 1946) and Dufourmentel (Dufourmentel, 1962), shown in Figure 1.3. Such variations give rise to two underlying questions: 1) which flap results in the best stress field; and 2) is there any better flap design (in terms of the stress field) other than the existing variations?

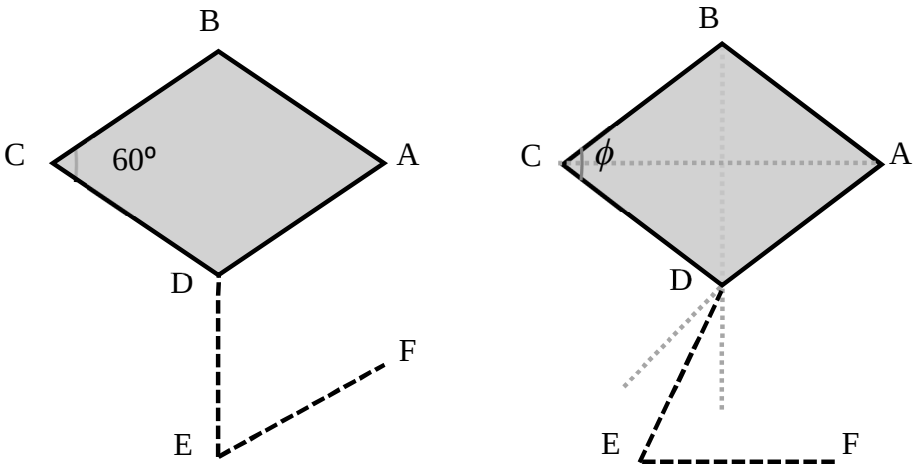

Figure 1.3 the flaps of Limberg (left) and Dufourmentel (right)

1.2. Structure of Skin

Skin, which is referred to as the *common integument*, covers the body with an average surface area of 1.7 m^2 in an adult (Faller et al., 2004). Also, this tissue has many derivatives (skin appendages) such as glands and sensory organs. A general schematic of skin is shown in Figure 1.4 with the whole tissue is divided into epidermis, dermis, and subcutaneous layer.

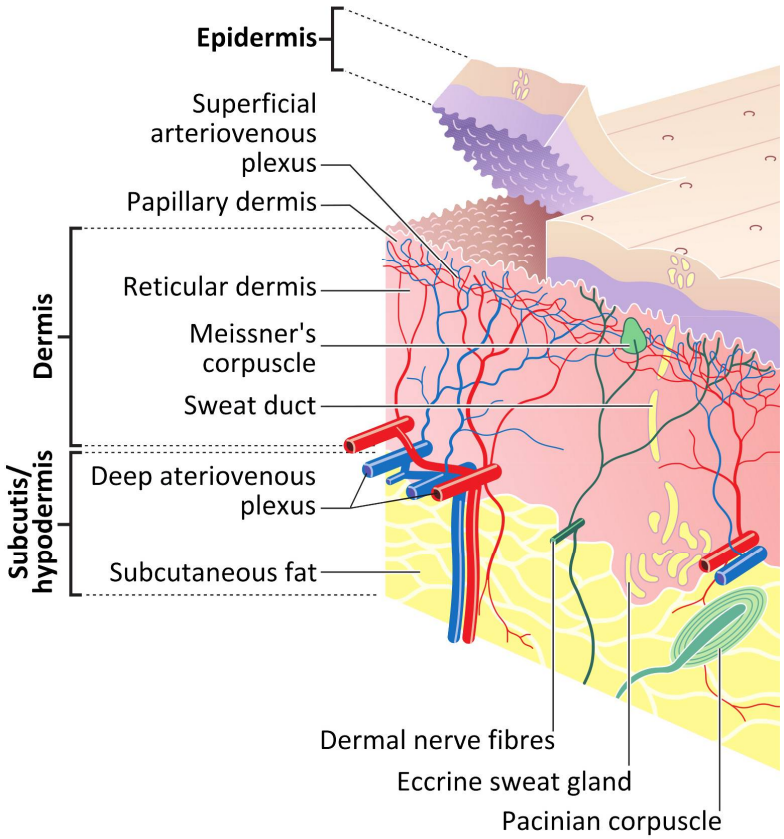

Figure 1.4 Structure of skin[2]

The epidermis is the outermost layer of skin and, in most regions of the body, has a thickness of 0.1 – 0.2 mm. The epidermis is mainly comprised of the keratinocytes cells and, based on different levels of keratin maturation from the lower layers towards the surface, is classified into four sublayers:

1) stratum basale (basal or germinativum cell layer) that is the innermost layer in the structure of epidermis and comprises both dividing and non-dividing keratinocytes;
2) stratum spinosum (spinous or prickle cell layer);
3) stratum granulosum (granular cell layer); and

[2] Madhero88 and M.Komorniczak, 2012. Available at: https://en.wikipedia.org/wiki/File:Skin_layers.png

4) stratum corneum (horny layer) that is the outermost layer of the epidermis (and skin) and encompasses fully matured keratinocyte.

Below the epidermis is the dermis layer which is comprised of a fibrous network of material. Based on different regions in the body, the thickness of dermis varies between 0.6 mm to 3.0 mm. This layer of skin is mainly comprised of 4 components:

1) As the main component of dermis, collagen fibers (approximately 70% of fat-free dry weight) form a wavy network which, despite irregularity, are almost parallel to skin layers (Brown, 1972). The width of each fiber is usually between 1 μm to 40 μm (Wilkes et al., 1973).
2) Elastin is the second major constitutent of dermis (almost 4% of fat-free dry weight) and is not as stiff as collagen. Width of elastin fibers varies between 0.5 μm to 8 μm (Wilkes et al., 1973).
3) Reticulin is another component which is so similar in molecular structure with collagen fibers and constitutes a relatively small portion of the dermis (almost 0.4% of fat-free dry weight).
4) Ground substance holds the fibrous network together.

Finally, cutis or the subcutaneous layer is the innermost part of skin tissue and is composed of loose connective tissue and fat. In flap surgery, usually the epidermis and dermis are detached from the subcutaneous tissue.

1.3. Mechanical Properties of Skin

Skin is a highly complex material and, as seen in Section 1.2, is non-homogeneous. It shows anisotropy, nonlinearity, and viscoelasticity. To provide more insight into the overall mechanical properties of skin, it is very helpful to understand the mechanical behavior of each component. As the outermost layer of skin, epidermis (and in paricular, stratum corneum) is the stiffest and the least extendable constituent of skin. Despite its relatively low level of viscoelastic behavior, epidermis has a nonlinear stress-strain behavior. Nevertheless, due to its small thickness, contribution of epidermis to the overall mechanical properties of skin is usually neglected (Wilkes et al., 1973). Since the results of mechanical tests on full thickness skin are almost similar to those of the dermal layer, the mechanical properties of skin is usually attributed to this part. In this regard, the key components of dermis, collagen and elastin, play a major part in the anisotropic stress-strain type of skin, and the ground substance adds to the viscoelasticity of the tissue.

To highlight the role of fiberous network in the dermis, a typical uniaxial in-plane stress-stretch relationship for human skin is illustrated in Figure 1.5. In Region I, most of the collagen fibers are not straightened and, therefore, the material is less stiff and there is not much resistance to an applied load. The dominant behavior of skin in this region is mostly attributed to the elastin fibers. In Region II, some of collagen fibers are straight and can carry load, hence a partial increase in stiffness. In Region III, almost all of them are along each other and increase stiffness (Daly, 1982).

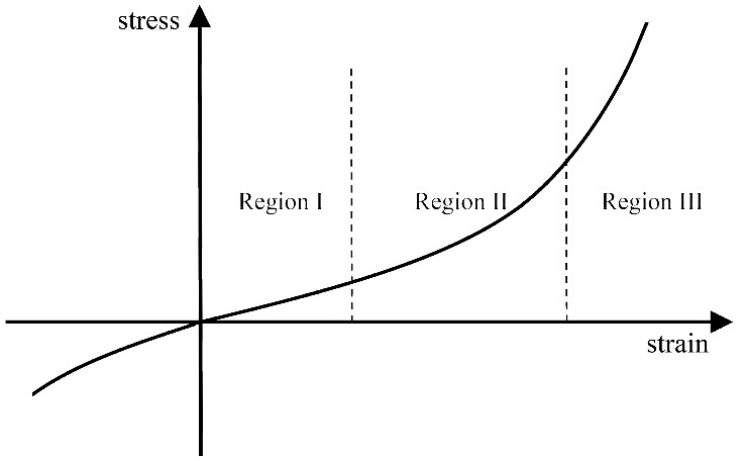

Figure 1.5 A typical uniaxial in-plane stress-stretch relationship for human skin

Skin's mechanical properties vary considerably and depend on many factors such as age (Daly and Odland, 1979; Escoffier et al., 1989), gender (Grahame, 1970; Seidenari et al., 1994), and race (Berardesca et al., 1991; Wilson et al., 1988). Regardless of such variations, not only skin's mechanical properties vary in different regions of one's body, but they are also different in various directions in a particular region of body. Such dependency on orientation was first reported by Langer (1978) who identified natural lines of tension in skin. He realized that if a circular hole is made in the skin of a cadaver, it would look like an elliptical shape. The orientation of Langer's lines, however, was seen sometimes to be different from the orientation of natural creases formed in living subjects. A number of variations have been proposed for the classical Langer's lines. The relaxed skin tension lines (RSTLs) (illustrated in Figure 1.6) are one common variation that are along the direction of greatest tensions in skin (Borges, 1984). The lines of maximum extensibility (LME) are at right angle with respect to RSTLs and represent an orientation in which wound closure causes the least tension (Borges, 1978).

Figure 1.6 Pattern of facial RSTLs (Patel and Sykes, 2011)[3]

Nonetheless, skin's elastic behavior (i.e. the ability of solid materials to return to their initial configuration when the load is removed) can be noticed with relatively small amounts of applied load, such as in region I of Figure 1.4. As the stress is increased, strain also becomes a function of time. This property is referred to as viscoelasticity and is commonly identified by creep and relaxation. Simply speaking, creep refers to continuous strain under a constant load; stress relaxation refers to reduction of stress under constant strain. Such time-dependent processes occur mainly due to displacement of interstitial fluid (that is loosly bound to the ground substance) as the collagen fibers are deformed. Creep and stress relaxation are of indespensible importance in

[3] Reprinted from Oper. Tech. Otolaryngol. - Head Neck Surg., 22, Patel, K.G., Sykes, J.M., Concepts in local flap design and classification, 13–23, Copyright (2015), with permission from Elsevier.

wound closure using skin flaps because they can alleviate the undesirable effects of intense stresses within a day (Reihsner and Menzel, 1998). However, although such properties can save a poorly designed/implemented flap, they should not be considered as design parameters in flap design (Larrabee and Bloom, 2007).

1.4. Use of Finite Element Method

Use of flaps for wound closure has its origin in 300 B.C. (Larrabee and Galt, 1986), and since then, this practice has been mostly based on practical experience (Danielson, 1978). As the first scientific attempt to investigate the tension created in local flaps, Limberg (1946) utilized paper models to devise a novel surgical procedure, i.e., the Limberg flap. To overcome some geometrical limitations imposed by the Limberg flap and to alleviate the tension effects, Dufourmentel (1962) proposed a modified version. After a comprehensive study on the Limberg and the Dufourmentel flaps, Lister and Gibson (1972) drew the conclusion that "the analysis and prediction of the exact behavior of either flap would require a computer rather than a plastic surgeon." In fact, biomechanics of wound closure, which is a key factor in flap design, could be much more accurately evaluated using virtual models. Since then, there has been considerable effort towards developing various models for biomechanics of flaps using FE. The FE model allows for robust, safe exploration into the expected outcomes for a wide range of geometries, including those that are proven to be unacceptable, without any risk to actual patients.

In one of the earliest cases, Larrabee (1986) modeled basic skin flaps, such as the rectangular advancement flap, using a simple FE model and rough meshing. This model was a good predictor of the general deformation field, but no convergence test was performed to evaluate the stress results (there were sharp corners in the model which could be a sign of stress singularity). Kawabata et al. (1989) used an anisotropic model for human skin. This model, however, was

developed by ignoring nonlinearities. They performed a series of virtual experiments for Z-plasty and obtained optimal patterns for this surgical technique which led to surgical recommendations. Deformation results were seen to be in good agreement with experiments; however, no convergence test for stress results was performed. This is important because there are extremely sharp corners in Z-plasty. Later, Pieper et al. (1995), presented a prototype computer program that included 3D model for skin of the human face. They used FE and incorporated a linear model. In this computer program, the results of deformation and tension could be estimated in wound closure. However, the model neglected to consider the nonlinear properties widely seen in soft tissues. Manios et al. (1996) made good use of FE and observed good agreement between the deformation results and the actual local skin flap procedure. The skin model, however, did not take into account material nonlinearities. Sharp corners, also, received no proper treatment to guarantee stress convergence. Chaudhry et al. (1998) conducted a study to find optimal patterns for suturing elliptical and triangular wounds. They considered human skin as an elastic material with an incremental moduli to estimate nonlinear effects. Yoshida et al. (2000) simulated three different methods of suturing for assessing dog-ear formation. To do this, they employed a 3D model of skin but neglected material nonlinearities. Later, Sifakis et al. (2009), based on an FE model, created a virtual surgical environment for suturing. Although they used a nonlinear constitutive model for skin, their model was limited to deformation prediction of deformation and for training purposes because rough elements were employed with no special attention to stress convergence. Flynn (2010) examined FE models of circular, elliptical, fusiform, and lazy-S plasty, and determined the optimal pattern. In addition to skin nonlinearities, he incorporated skin anisotropy using an orthotropic hyperelastic constitutive model. No sharp corners were included in the modeled sututing methods and stress convegence was addressed. A year after, Capek et al.

(2011) concluded that some geometric optimizations could be applied to the Limberg flap. Without revealing much information about the model, they mentioned that implementing the rhombic flap with lower incision angles would bring about lower tension (which is in contrary with the results obtained in the current study). Pauchot (2012) developed an FE model to simulate V-Y advancement flaps. They used a nonlinear material model but the meshing did not appear to guarantee stress convergence due to the presence of very sharp corners. Buganza-Tepole et al. (2014) developed an FE model to assess the direct advancement flap and the double back-cut flap, and they noted that FE has the potential for optimization of skin flap design. In their study, a 3D model featuring an anisotropic material model was used. Topp et al. (2014) also studied a number of rhombic flaps using FE and discussed the optimized designs. They employed a nonlinear hyperelastic material model. In their model, and the optimal pattern was selected by considering a relatively small number of flap candidates[4].

In most of the studies on FE models of wound closure in the literature, boundary conditions are modeled where either the defects to be closed are symmetric or the post-surgical shape of scars are constrained, such as in (Chaudhry et al., 1998; Flynn, 2010; Pauchot et al., 2012). Although this can result in a considerable computational simplification, the resulting FE model may not predict true deformation for more complex wounds, hence adding to inaccuracy in estimating the tension field. In more recent studies, however, there have been a number of cases in which improvements were applied to rectify shortcomings (Buganza-Tepole et al., 2014; Sifakis et al., 2009; Topp et al., 2014).

[4] In my research, I started off with a geometry almost identical to that in Topp et al. (2014). However, due to the presence of sharp corners, stress convergence could not be achieved. I noticed that stress values unlimitedly diverged as the sizes of elements were decreased. Of note, stress singularity is a frequent issue in FE models and is well described in many text books such as in Gladwell (1980).

Moreover, each of the comparative studies on wound closure (Flynn, 2010; Kawabata et al., 1989; Lott-Crumpler and Chaudhry, 2001; Topp et al., 2014) has been performed by considering only one material model whereas the mechanical properties of skin varies considerably. Such uncertainties, coupled with the intrinsic material nonlinearities of skin, can alter the outcome of a comparative study to a great extent if only one material model is employed.

1.5. Objective and Methodology

As a general objective, this research seeks to create an optimized design for the rhombic transposition flap. The optimization is centered on minimization of the maximum von Mises stress with constraints on maximum compressive stress and deformation. To accomplish this goal, my MSc research was planned in three phases:

1) An FE model for simulating complex wound closure was developed. In this regard, it was necessary to create a reliable constitutive model for skin tissue by means of applying principles of hyperelastic modelling. The quantitative data describing the mechanical properties of skin were adapted from the literature from different experiments on human subjects. Additionally, there was a need to develop a reliable method of simulating sutures as they behave in reality. The modelling tool for wound closure developed in this phase could be of great use to simulate almost any technique of wound closure in plastic surgery.
2) Virtual experiments (by computer simulation) on a wide variety of rhombic flaps with various configurations were performed. These incorporated a robust set of geometries and tissue properties to allow for the study of skin in different regions of the body and in different individuals. The sets of geometries were based on variations of the rhombic transposition flaps used in current surgical practice and described in the literature

review (Section 1.4). The simulations were implemented through a detailed computer code that was written within a commercially available FE package (ANSYS®).

3) Analysis and interpretation of the results were performed to determine an optimized design. The stress (von Mises stress and principal components of the Cauchy stress) and deformation results were analyzed for different configurations and material models. In this phase, also, the effects of uncertainties associated with the mechanical properties of skin were investigated.

1.6. Organization of Thesis

This thesis was adapted from two manuscripts. In Chapter 2, to provide a general insight into the underlying theories behind the subject, the pertinent basics of continuum mechanics are presented. Chapter 3 (adapted from the first manuscript) outlines detailed information concerning a new FE model of wound closure, including the parametric geometry, meshing, and material modeling. As test cases, the flaps of Limberg and Dufourmentel are modeled, and the results are compared to reported observations with surgery. Chapter 4 (adapted from the second manuscript) applies my new FE model to identify an optimized design of the rhombic transposition flap. Chapter 5 presents a concise summary of objectives and conclusions.

2. Theory

2.1. Introduction to Kinematics

2.1.1. Configurations

From a precise physical point of view, down to the molecular level, the structure of skin is quite complex, and its exact mechanical behavior would require highly sophisticated computations. However, it has been widely accepted that a continuum model can reasonably account for its behavior, both in terms of kinematics (geometry of deformation) and its kinetics (force and stress distributions). A continuum body includes an infinite number of material points whose simultaneous position set is called a configuration. The reference configuration includes the position of each point, $\boldsymbol{X}$, within the real continuous space at some instant in time, t. On the other hand, when an object undergoes a deformation, the current configuration includes the new position, $\boldsymbol{x}$, of each of the material points. The reference and current configurations can be related to each other using a deformation map so that

$$\boldsymbol{x} = \boldsymbol{x}(\boldsymbol{X}, t). \tag{2.1}$$

It should be noted that both $\boldsymbol{X}$ and $\boldsymbol{x}$ are vector parameters.

2.1.2. Deformation Gradient

The relative displacement existing between the material points is commonly measured by means of the deformation gradient $\boldsymbol{F}$ such that

$$\boldsymbol{F}(\boldsymbol{X}, t) = \frac{\partial \boldsymbol{x}(\boldsymbol{X}, t)}{\partial \boldsymbol{X}}. \tag{2.2}$$

Therefore the line elements $d\boldsymbol{x}$ and $d\boldsymbol{X}$ can be related to each other by

$$d\boldsymbol{x} = \boldsymbol{F}\, d\boldsymbol{X}\,. \tag{2.3}$$

Using Einstein's indicial notation, the components of the deformation gradient tensor are then specified as

$$F_{ij} = \frac{\partial x_i}{\partial X_j}. \tag{2.4}$$

As an object undergoes a deformation, there may occur local changes in volume. Assuming $dV_{\boldsymbol{X}}$ and $dV_{\boldsymbol{x}}$ as the volume of an infinitesimal cube in the reference and the current configurations, respectively, it can be shown that

$$\det \boldsymbol{F} = \frac{dV_{\boldsymbol{x}}}{dV_{\mathrm{X}}}. \tag{2.5}$$

For any isochoric deformation, similar to the deformation associated with nearly incompressible materials such as skin and other soft tissues, the deformation gradient is such that $\det\boldsymbol{F} = 1$.

2.1.3. Polar Decomposition of the Deformation Gradient

For any strain measure, there should be no strain when a continuum body experiences rigid body motion. Therefore it is useful to separate the deformation gradient into two tensors: an orthogonal tensor $\boldsymbol{R}$ which is dependent on the rotation at the physical point of interest, and a symmetric tensor $\boldsymbol{U}$ which is independent of rotation, so that

$$\boldsymbol{F} = \boldsymbol{R}\boldsymbol{U}\,. \tag{2.6}$$

$\boldsymbol{R}$ is called the rotation tensor and $\boldsymbol{U}$ is the right stretch tensor. It is the right stretch tensor $\boldsymbol{U}$ which defines the stress-related deformation at each point in the body. In many analyses, including those in the present research (Chapters 3 and 4), the deformation is described in terms of the eigenvalues λ_i of $\boldsymbol{U}$, also called the principal stretches. The principal stretches λ_i are given by

$$\Lambda = \boldsymbol{Q}^T \boldsymbol{U} \boldsymbol{Q}. \tag{2.7}$$

$\boldsymbol{Q}$ is the tensor providing the coordinate transformation to the principal directions of tensor $\boldsymbol{U}$.

2.1.4. Green Strain Tensor

In addition to describing the deformation in terms of principal stretches λ_i, the analysis of stress and strain to follow in Chapter 3 also refers to the Green Strain Tensor. Using the polar decomposition given in (2.6), the right Cauchy deformation tensor $\boldsymbol{C}$ is first defined, and can be written as

$$\boldsymbol{C} = \boldsymbol{U}^2 = \boldsymbol{F}^{\mathrm{T}} \boldsymbol{F} . \tag{2.8}$$

Then, the Green strain, also referred to as the Lagrangian strain tensor, is defined as

$$\boldsymbol{E} = \frac{1}{2}\left(\boldsymbol{C} - \mathbf{I}\right), \tag{2.9}$$

where $\mathbf{I}$ is the identity matrix. Note that, as required, the definition of $\boldsymbol{E}$ ensures that the strain is zero in the absence of deformation; i.e., when $\boldsymbol{C} = \mathbf{I}$.

2.2. Stress Tensor

2.2.1. Cauchy Stress Tensor

The Cauchy stress tensor, also known as the true stress tensor, completely defines the state of stress at a material point in the current configuration. Figure 2.1(a) shows the instantaneous force vector, $\boldsymbol{df}_x$, acting on an infinitesimal area, dA_x, with outward unit normal vector, $\boldsymbol{n}_x$ in the current configuration. The corresponding infinitesimal area, dA_X, surface normal, $\boldsymbol{n}_X$, and the transformed instantaneous force, $\boldsymbol{df}_X$, which are all in the reference configuration, are also shown in Figure 2.1(b).

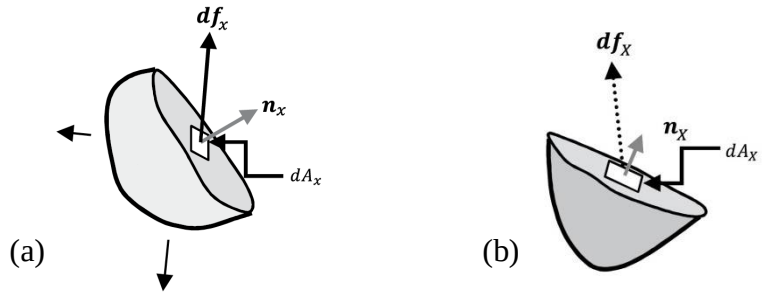

Figure 2.1 Internal forces, surface normal and infinitesimal area in (a) current, and (b) reference configurations. From Capaldi (2012).

The Cauchy stress tensor, $\boldsymbol{\sigma}$, is obtained by

$$\boldsymbol{df}_x = \boldsymbol{\sigma}^T \boldsymbol{dA}_x , \tag{2.10}$$

where $\boldsymbol{dA}_x = dA_x \boldsymbol{n}_x$ and (2.10) relates the forces and areas in the current configuration, i.e. $\boldsymbol{df}_x$ and dA_x. It is the Cauchy stress tensor that will be used in the final assessment of the stress distributions in skin, whether in terms of principal values or in determining the von Mises stresses.

2.2.2. First Piola-Kirchhoff Stress and the Nominal Stress

Although the Cauchy stress (or true stress) is used in final assessments (such as in optimizing flap geometry), other stress measures are also important in that they are often used in defining material (stress-strain) properties. The First Piola-Kirchhoff stress $\boldsymbol{P}$ is defined so that it relates the force in the current reference ($\boldsymbol{df}_x$) to the referential area (dA_X), i.e.

$$\boldsymbol{df}_x = \boldsymbol{P}^T \boldsymbol{dA}_X . \tag{2.11}$$

where $\boldsymbol{dA}_X = dA_X \boldsymbol{n}_X$. The relation between this stress measure and the Cauchy stress can be determined by

$$\boldsymbol{P} = \left(\det \boldsymbol{F}\right) \boldsymbol{F}^{-1} \boldsymbol{\sigma} . \tag{2.12}$$

It should be noted that $\boldsymbol{P}$ is not a symmetric tensor. In the case of a tension test, the magnitude of $\boldsymbol{P}$ is equivalent to what is usually called the engineering stress. The "nominal stress tensor", which

is commonly used in the literature for reporting the results of stress-stretch tests for defining skin properties can be also defined, and is the transpose of the first Piola-Kirchhoff stress.

2.2.3. Second Piola-Kirchhoff Stress and Work Conjugates

There is also an imaginary stress measure, known as the second Piola-Kirchhoff stress, which is important for its relation to Green's strain when applying the energy methods associated with material properties and finite element analysis. It defines a fictitious force obtained by applying the inverse deformation gradient to the current force. This fictitious force is related to the area in the reference configuration. Mathematically, the second Piola-Kirchhoff stress tensor **S** can be obtained by

$$\boldsymbol{F}^{-1}\boldsymbol{df}_x = \boldsymbol{S}^T \boldsymbol{dA}_X \,. \tag{2.13}$$

The advantage of using this imaginary stress tensor is that the second Piola-Kirchhoff stress and the Green strain are work conjugates. Therefore, $\boldsymbol{S}$ can be calculated using

$$\boldsymbol{S} = \frac{\partial W_0}{\partial \boldsymbol{E}}, \tag{2.14}$$

where W_0 is the strain energy function per unit volume in the reference configuration.

2.3. Hyperelasticity

Hyperelasticity is a type of constitutive modeling for ideally elastic material when subjected to very large strains, and takes into consideration both material and geometric nonlinearities. In this theory, rather than writing a direct relationship between the stress and strain components (such as in generalized Hooke's law), a general form for W_0 is considered so as to map the Green strain to the second Piola-Kirchhoff stress using (2.14).

3. Finite Element Simulation of Local Flaps in Plastic Surgery

3.1. Synopsis

This chapter was adapted from a manuscript entitled "Finite Element Simulation of Local Flaps in Plastic Surgery", which my co-author, Professor Allan T. Dolovich, and I prepared for publication. Professor Dolovich provided a supervisory role in defining the problem, providing useful information and discussion, and revising the manuscript. My contribution to this manuscript was that I wrote the FE code within ANSYS, obtained the results, provided a significant part of the discussion, and prepared the draft of the manuscript.

3.2. Objective

The objective of this work was to create a reliable finite element framework for simulation of wound closure. This paper provides detailed information concerning the new FE model, including the parametric geometry, meshing, and material modelling. As test cases, the flaps of Limberg and Dufourmentel were modeled, and the results were compared to the reported observations in real surgeries.

3.3. Methods

3.3.1. Rhombic Transposition Flaps

A typical rhombic transposition flap is illustrated in Figure 3.1(a). To construct such a flap, first, the lesion is excised so that a rhombic area ABCD with an acute angle ϕ is created. Then, the flap is constructed by creating two more incisions, first from D to E at an angle θ_1 measured

from an imaginary line extending from the short diagonal BD, and then a second incision from E to F at an angle θ_2 with respect to ED. All the sides of the defect and the added incisions have the same length. The common choice of direction for implementing the flap is usually made by considering relaxed skin tension lines (RSTL) (Borges, 1984, 1978) which are related to directional properties of skin.

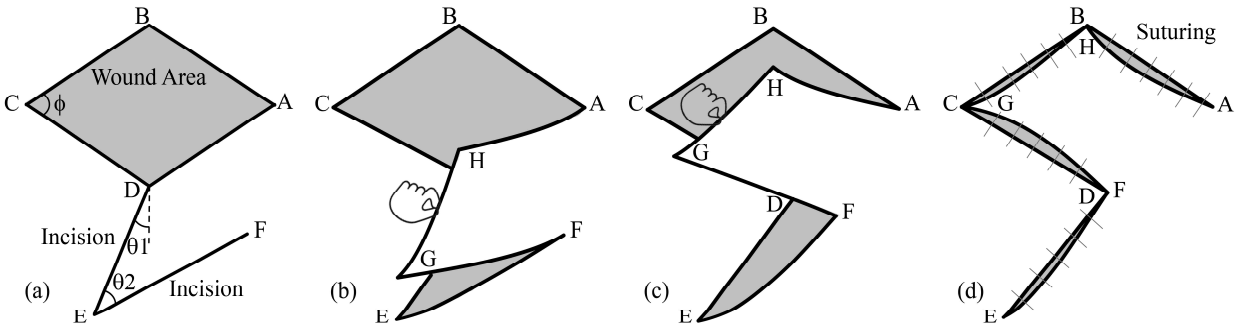

Figure 3.1 The process of wound closure using a typical rhombic flap (left to right)

If ϕ = 60°, θ_1 = 0°, and θ_2 = 60°, the rhombic flap is called the Limberg flap (shown in Figure 1.3). The Dufourmentel flap is constructed with ϕ having any value between 60° and 90°, incision DE bisecting the imaginary extensions of BD and AD (so that θ_1 is equal to half the angle between these extensions), and θ_2 is defined so that the last incision EF is parallel to the long diagonal CA of the rhombic defect. That is, the angles in the Dufourmentel flap are given by $\theta_1 = 45° - \phi/4$ and $\theta_2 = 45° + \phi/4$ (shown in Figure 1.3).

After creating the flap, it should be transposed so that the defect is filled and the edges of the flap and defect are placed along each other to facilitate proper suturing. To do this, as shown in Figure 3.1, the created flap FGHA is undermined and is pulled over the defect to ease the process of wound closure.

3.3.2. Finite Element Simulation

The development of the FE model was performed through a detailed parametric computer code written within a commercially available FE package (ANSYS®). A planar model with the assumption of plane-stress was employed.

3.3.2.1. Modeling Skin

To model human skin, in general, one may consider different aspects such as nonlinearity, anisotropy, and viscoelasticity. The model here incorporates large deformation and its associated geometric nonlinearity, and assumes a nonlinear hyperelastic constitutive model as a representation of the skin's behavior. Since this research focused on wound closure processes occurring over relatively short periods of time, time-dependent effects such as stress-relaxation were neglected. This is a common assumption in previous research where the constitutive properties of skin have been accurately modeled for loadings of similar duration (Jor et al., 2011; Kirby et al., 1998; Lapeer et al., 2010; Ní Annaidh et al., 2012). In addition, for the modelling and comparisons presented here, it was assumed that the skin properties are isotropic. This assumption was made to focus, in this first instance, on the geometric effects of large deformation and the consequences of nonlinear material behavior, without introducing additional directional variables resulting from anisotropy (whether it be in the form of transverse isotropy due to skin layering, or a more detailed anisotropic model). This allowed for investigation into whether FE analysis of local flaps showed promise.

As widely seen in the literature (Gennisson et al. (2004), Ní Annaidh et al. (2012)), a typical stress-strain relationship for skin in a simple tension-compression test can be plotted as shown in Figure 3.2 where the nominal stress N is plotted in terms of stretch λ. (By definition, the nominal

stress tensor ***N*** is defined as the transpose of the first Piola-Kirchhoff stress, and the stretch refers to the ratio of final length to initial length of a line element. In the context of Figure 3.2, the stress refers to a single component of ***N***, namely $N = N_{11}$.)

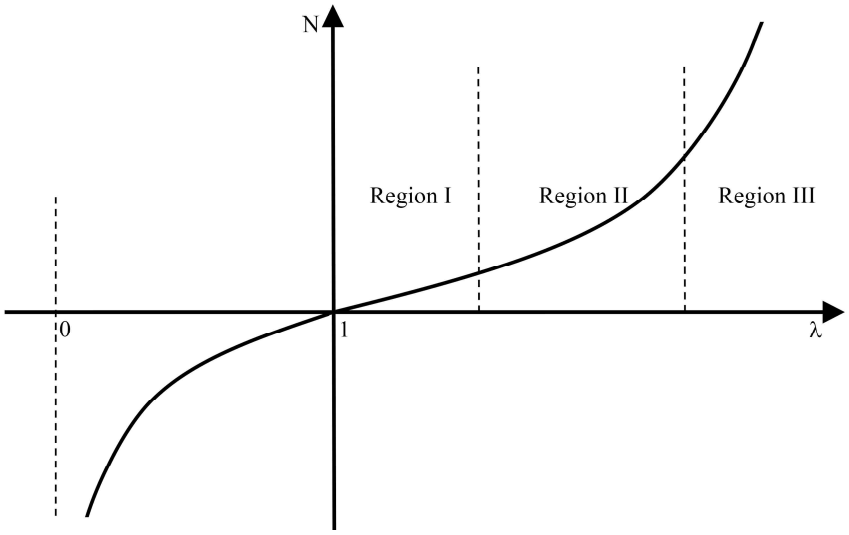

Figure 3.2 A typical uniaxial in-plane stress-stretch relationship for human skin. The nonlinear behavior of skin is attributed to the combination of elastin with collagen fibers. In Region I, most of the fibers are not straightened. In Region II, some of them are straight, and in Region III, all of the fibers are along each other and cause further stiffness (Daly, 1982).

To incorporate this material behavior using hyperelastic modelling, a set of criteria was applied. First, to have a stable relation, the curve was required to remain in the first and third quadrants for the tension and compression parts, respectively. This was needed because, if curve-fitting was accomplished by only considering data in the tension part, it could result in unstable, inaccurate, and/or nonphysical results for the numerical modelling of compression. However, in the case of skin modeling, it is often the case that only tensile uniaxial data are employed in the simulation of biaxial loading. Here, in this study, to avert this difficulty, an inflection point was considered at the origin, i.e., $d^2N/d\lambda^2 = 0$ at $(\lambda, N) = (1, 0)$. Making certain that the initial slope was positive and the function $N(\lambda)$ increased everywhere guaranteed this desired stability. In

addition, assuming in-plane deformation, the compressive stress should reach a high level when the stretch ratio approaches zero. To implement this fact here, $\lambda = 0$ is theoretically considered as a vertical asymptote for the curve, i.e. $\lim N = -\infty$ as $\lambda \to 0^+$.

Taking into account the qualitative criteria just outlined, a two-term Ogden hyperelastic model (Ogden, 1997, 1972) was employed, with the strain energy density function W_0 expressed in terms of the principal stretches λ_1, λ_2, and λ_3 such that

$$W_0 = \sum_{p=1}^{2} \frac{\mu_p}{\alpha_p} \left(\lambda_1^{\alpha_p} + \lambda_2^{\alpha_p} + \lambda_3^{\alpha_p} - 3 \right), \tag{3.1}$$

where μ_p and α_p are material constants. For uniaxial tests and assuming skin to be an isotropic and incompressible material, it can be shown that:

$$\lambda_1 = \lambda_2^{-2} = \lambda_3^{-2} = \lambda \,. \tag{3.2}$$

Using (3.1) and (3.2), the first principal component of nominal stress N_{11} is then derived as

$$N_{11} = \lambda \frac{\partial W_0}{\partial E_{11}} = \sum_{p=1}^{2} \mu_p \left(\lambda^{\alpha_p - 1} - \lambda^{-\frac{\alpha_p}{2} - 1} \right), \tag{3.3}$$

where E_{11} is the first component of the Green strain and, in this case, $E_{11} = (\lambda^2 - 1)/2$. By adapting data from Ní Annaidh et al. (2012), the initial slope (Region I in Figure 3.2) and final slope (Region III in Figure 3.2) were considered to be 1 MPa and 88 MPa, respectively, and a data point in Region III (λ, N)=(2, 20 MPa) was assigned. Using these values, the coefficients μ_1, μ_2, α_1, and α_2 were then estimated to be 0.0439 MPa, - 0.236 MPa, 9.82, and -1.00 respectively. The resulting stress-stretch relationship of the defined material is shown in Figure 3.3.

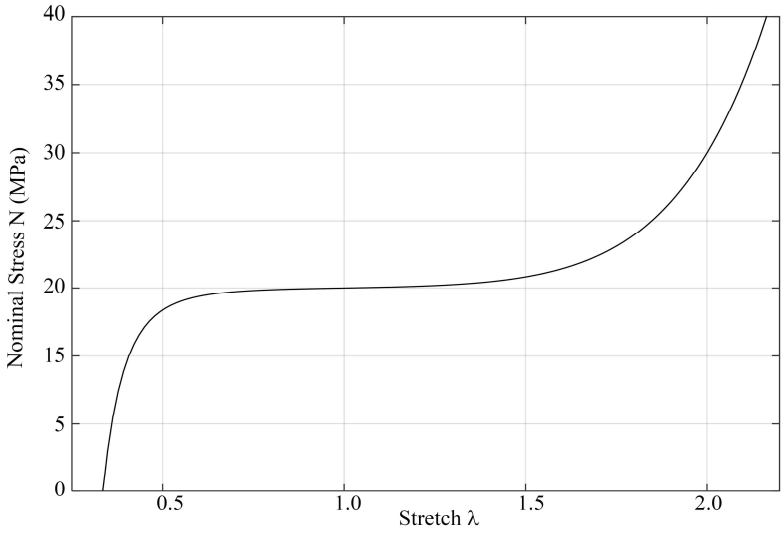

Figure 3.3 The stress-stretch behavior of the material used in this research in a uniaxial in-plane loading

3.3.2.2. Geometric Model and Meshing

The geometric model together with the applied meshing is shown in Figure 3.4, where all the sides of the defect and flap have the same length (30 mm), the outer circular boundary having a diameter of 300 mm, and the thickness (in the direction perpendicular to the plane of the model) being 1.5 mm (skin thickness varies with location in the body, and the value considered here is based on the average amounts reported in Groves et al. (2013) and Reihsner et al. (1995)). To achieve a balance between accuracy (in terms of mesh refinement) and computational expense, a small gap of 0.60 mm was selected for the incisions. To avoid the issue of stress singularity (Danielson, 1978), some corners were made round. Due to the irregular form of the model, triangular elements were defined, and midpoint nodes were added to provide high accuracy (this was important because, in the presence of bending loads, use of triangular elements without midpoints could lead to fallacious outcomes).

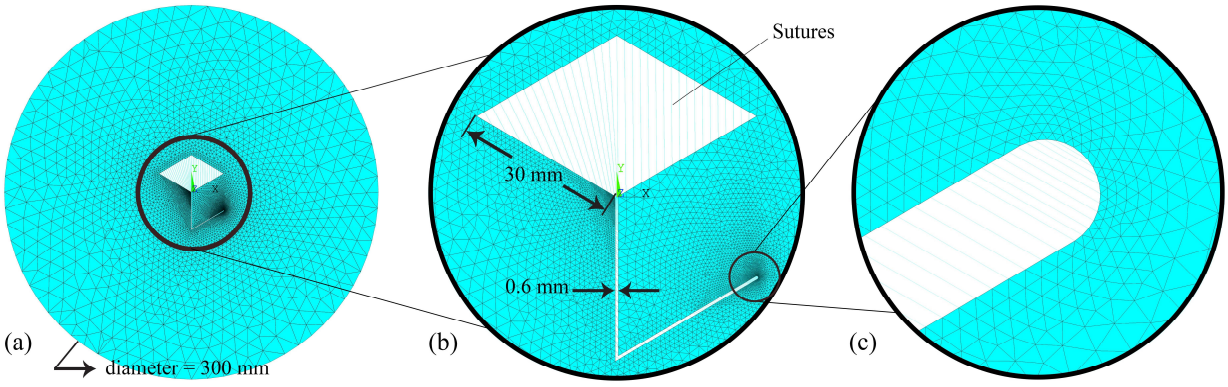

Figure 3.4 Geometrical modeling and meshing

3.3.2.3. Boundary Conditions and Loads

To simulate wound closure, sutures were modeled as two-force members with an "imaginary" material capable of undergoing large thermal strains. This approach allowed the sides of the wound to come together by applying an initial temperature above the ambient temperature, which then shrunk the members as they cool. It is important to note that the use of thermal effects is a means to model the suturing process — there is no actual temperature change with the surgical procedure, this is simply a creative modelling approach. In the model, all sutures had the same coefficient of thermal expansion α_{th}, the same elastic modulus E, the same cross-sectional area A, and all were subjected to the same temperature change ΔT. The parameter selection for α_{th}, E, and ΔT was made to achieve a balance between accuracy and computational expense associated with step-wise nonlinear modelling. To ensure that the shrinkage of sutures was not stopped by any opposing force applied by the tissue, the product of E and A was chosen to be sufficiently large (i.e. the sutures were quite stiff). The selected values were EA =1.00 MPa.m^2 and $\varepsilon_{th} = \alpha_{th} \Delta T$= -3.30, where ε_{th} refers to thermal strain.

To study the effects of skin's intrinsic pre-stress, the simulation was performed with and without the existence of pre-stress. Using the data from Jong (1995), the skin prestress

(compressive) was considered to be 0.0090 MPa and 0.024 MPa along the direction from F to D (as illustrated in Fig. 3.1(a)) and the direction perpendicular to it, respectively. Additionally, the outer circular boundary was fixed and plane stress theory was applied.

3.4. Results

3.4.1. Convergence

Using the geometric model and applied meshing, displacement and force convergence was successfully achieved. Figure 3.5 shows a plot of the maximum von-Mises stress (which almost always occurs at point F) with respect to the number of elements. Approximately 12,000 elements, in total, were required to achieve sufficient convergence for the purpose of my comparative study.

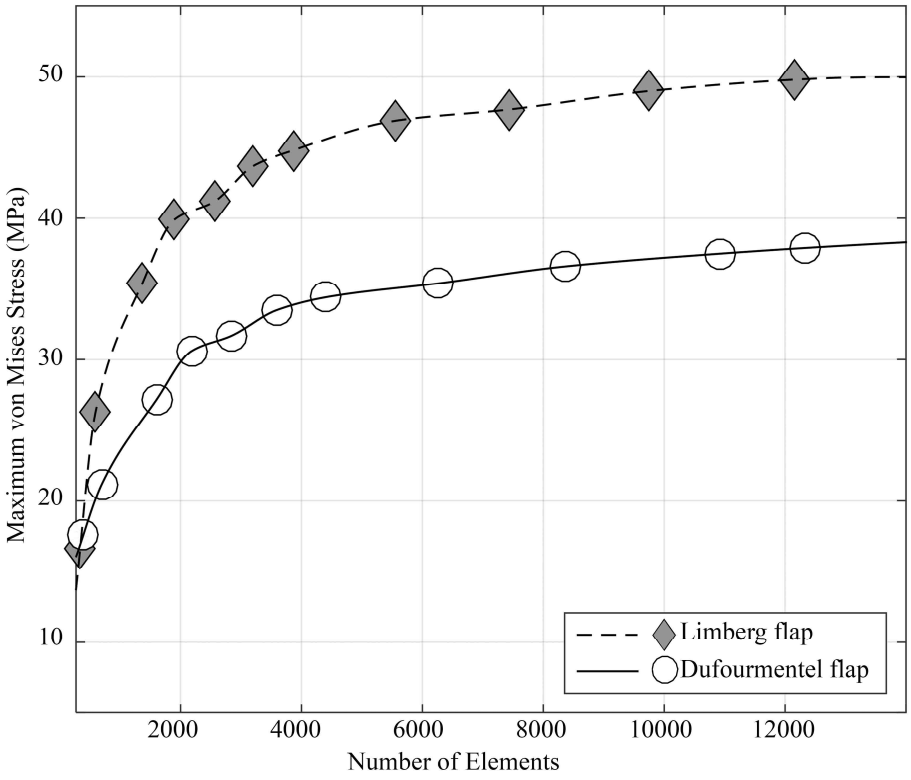

Figure 3.5 Convergence test for the Limberg and Dufourmentel flaps

3.4.2. Deformation

The step-by-step deformation results for the Limberg flap and the Dufourmentel flap (considering $\phi = 60°$) are shown in Figure 3.6 and Figure 3.7, respectively. To model the process of wound closure, each suture underwent a stretch of 0.037 (which corresponded to a logarithmic strain of - 3.30).

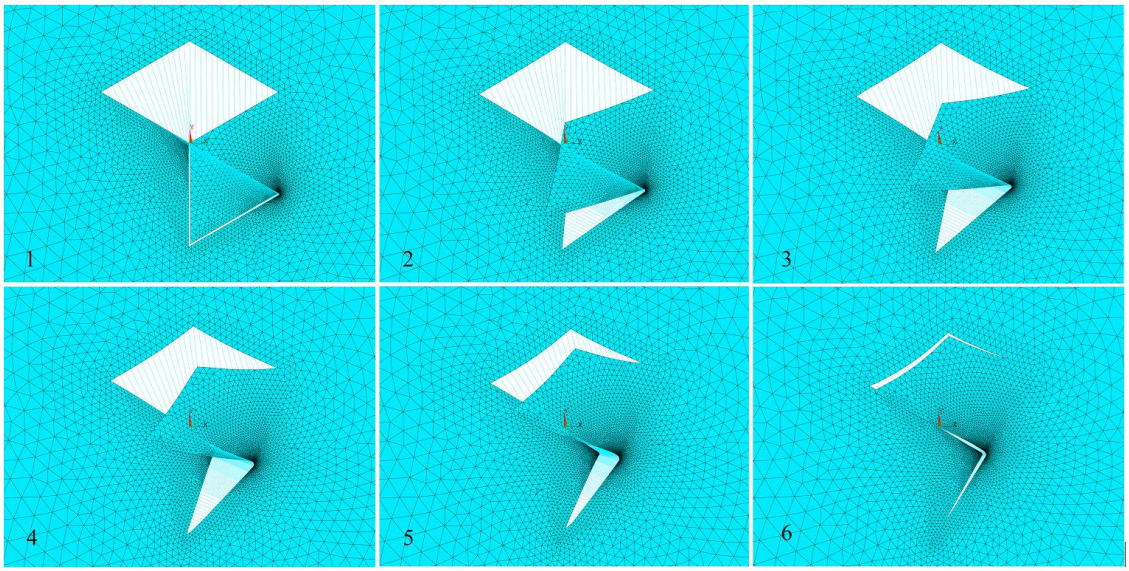

Figure 3.6 Simulated deformation of the Limberg flap

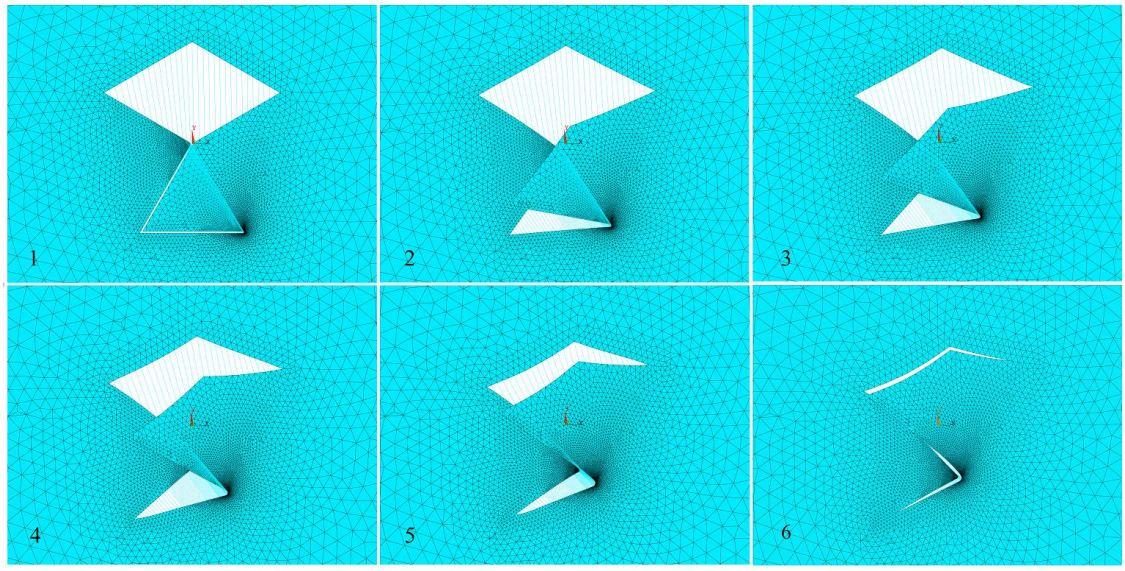

Figure 3.7 Simulated deformation of the Dufourmentel flap considering a 60° defect

Figure 3.8 shows the deformation results for the flaps of Limberg and Dufourmentel as they are compared to those of real surgeries. As can be seen, the proposed modeling approach can be a good predictor of the deformation for rhombic flaps.

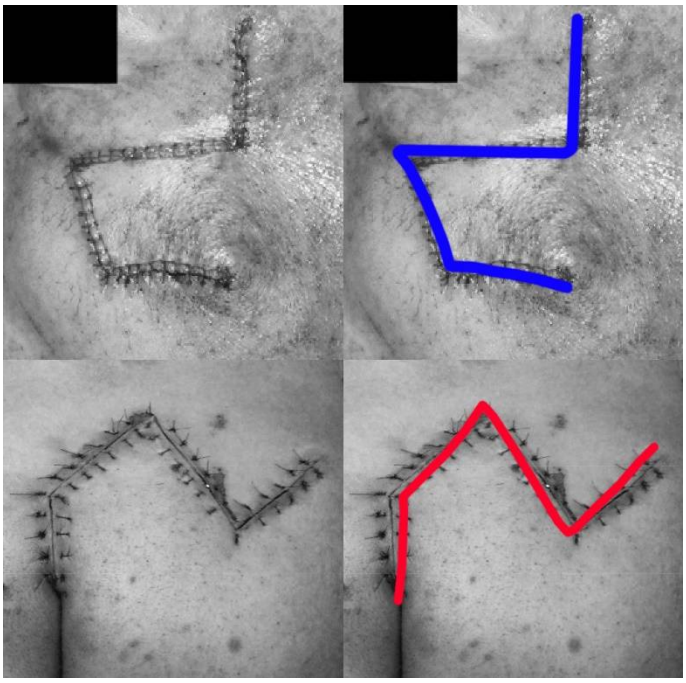

Figure 3.8 Comparisons between simulated deformations (specified with colored lines) and results from real surgeries: the Limberg flap (adapted from Furr and Wang (2011))[1] (top); and the Dufourmentel flap (adapted from Uraiqat (2010) with permission) (bottom)

3.4.3. Stress

The stress contours for the flaps of Limberg and Dufourmentel are shown in Figure 3.9. The maximum stresses in X and Y direction plus the von-Mises stresses for the Limberg flap were 22.1, 39.5, and 49.0 MPa, respectively. For the Dufourmentel flap, the stresses were less, with

[1] Reprinted from Oper. Tech. Otolaryngol. - Head Neck Surg., 22, Furr, M.C., Wang, T.D., Complex local flap design in cheek reconstruction, 53-58, Copyright (2015), with permission from Elsevier.

6.1, 36.3, and 37.5 MPa, respectively. The maximum compressive principal stresses in both the Limberg flap and the Dufourmentel flap were also approximately 0.50 MPa. The effect of pre-stress was found to be approximately 0.70 MPa in the von-Mises stress (less than 2% of the maximum von Mises stresses).

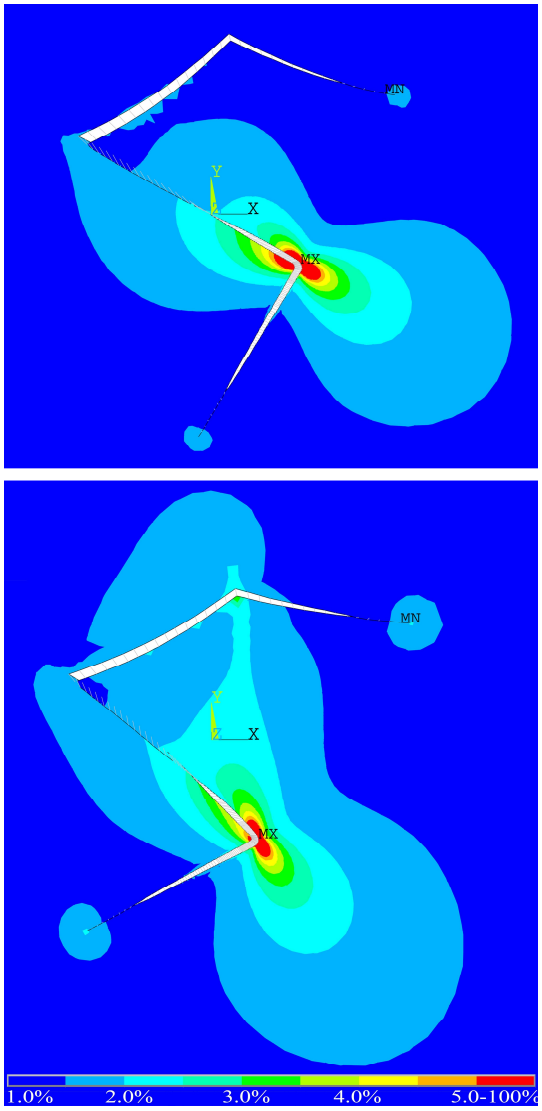

Figure 3.9 Contour plots showing the relative von-Mises stress distributions (with respect to the maximum values): the Limberg flap with maximum stress of 49.0 MPa (top), and the Dufourmentel flap with maximum stress of 37.5 MPa (bottom)

3.5. Discussion

At the initial stages of this research, we employed a relatively simple model which incorporated sharp corners. Despite good accuracy in predicting deformation, it led to non-convergent stress results due to stress singularities at some of the sharp corners. As an improvement, we developed the model presented here which featured enhanced geometry/meshing and showed convergence for both displacement and stress.

Although, even at 14,000 elements, stress values were still changing in each curve as they converged to their limits, the important quantity in a comparative study is the *difference* in stress between the two flaps. As can be seen in Figure 3.10, after the early signs of convergence become evident (beyond 8,000 elements), the difference in maximum von Mises stress, defined by

$$\sigma_d = (\sigma_{\max})_{Limberg} - (\sigma_{\max})_{Dufourmentel}$$

remained almost constant, where $\sigma_{\max}$ is the maximum von Mises stress. Therefore, by considering the convergence behavior of the model, fewer number of elements may be required in this comparative study, or other comparative studies, leading to optimal design.

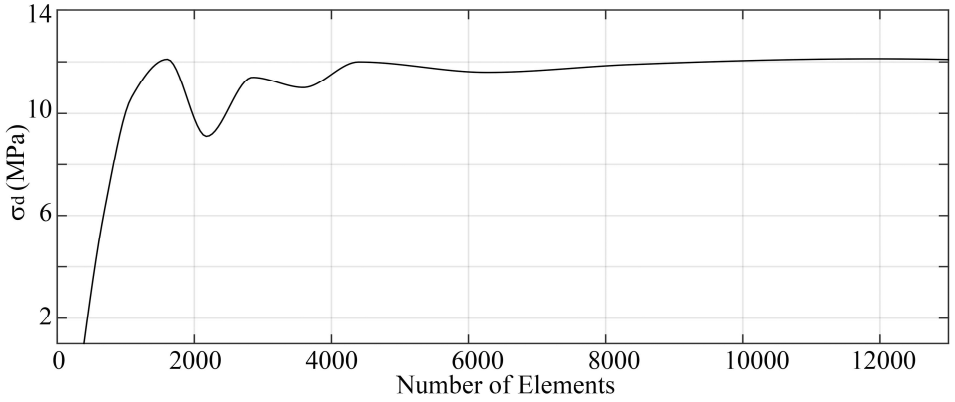

Figure 3.10 Relation between the difference in maximum von Mises stresses (in the flaps of Limberg and Dufourmentel) and the number of elements

Our use of thermal contraction for wound closure modeling proved to be an effective method for modeling wound closure. By using a single value of strain for all of the sutures, the gaps in the final configurations were created by uniform scaling. Although one could easily consider larger magnitudes of the thermal strain to create extremely small gaps, it would not markedly affect the final quantitative results, and would lead to more computationally expensive simulations.

As a result of applying compression, skin, in reality, undergoes out-of-plane deformation in the form of wrinkles or depressed areas. In this model, the assumption of in-plane deformation precludes such deformations, and instead creates compression points. Investigation of such points shows that the maximum compressive stress is small (roughly 1% of the maximum von-Mises stress in either model). The corresponding locations are also found to be far enough from the locations of interest where high magnitudes of tensile stress occur. Therefore, even though the planar model represents a simplification of reality, it appears to be reasonable for the purposes of this study.

Results of maximum stress location were in total agreement with the reported observations of real surgeries (Borges, 1978; Lister and Gibson, 1972; Mathew et al., 2008; McNay et al., 1997; O'Brien et al., 1976; Quaba and Sommerlad, 1987). Also, the simulation of the Dufourmentel flap revealed that its maximum von-Mises stress is 23% less than that of the Limberg flap, and that its stress field was distributed more uniformly. This result was consistent with the premise that the Dufourmentel flap is commonly regarded as an improved version of the Limberg flap.

Our results indicate that, due to the relatively small effect of prestress on the maximum stress, the prestress can be neglected from the simulations. The most noticeable impact of prestress was determined right after undermining the flap and before applying suture forces. At this point, due to the relatively low elastic modulus, the flap and sides of the defect underwent shrinkage.

It is important to note that, in our model, we considered only the elastic part of the stress-strain behavior. In reality, however, as a result of stress relaxation, the high stress associated with surgery will be considerably alleviated within a few hours (Reihsner and Menzel, 1998). However, loss of elasticity, particularly in aged skins, will be probably evident after such stress relaxations (Daly and Odland, 1979).

In conclusion, the developed FE model was observed to have a reliable performance; the skin model showed a stable behavior; the calculations were converged, and the stress/deformation results were in agreement with observations with real surgery. As presented in Chapter 4, the developed FE model was then used as a framework for performing virtual experiments to determine an optimized design.

4. From the Rhombic Transposition Flap Toward Z-plasty: an Optimized Design Using the Finite Element Method

4.1. Synopsis

This chapter was adapted from a manuscript, entitled "From the Rhombic Transposition Flap Toward Z-plasty: an Optimized Design Using the Finite Element Method", which my co-author, Professor Allan T. Dolovich, and I had submitted to the Journal of Biomechanics on May 12, 2015. The current status is "Under Review". Professor Dolovich provided a supervisory role in defining the problem, providing useful information and discussion, and revising the manuscript. As my major contribution to this manuscript, I wrote the FE code within ANSYS, obtained the results, provided some part of discussion, and prepared the draft of the manuscript.

4.2. Objective

The objective of this work was to design an optimized version of rhombic transposition flaps by minimization of maximum von Mises stress with constraints on maximum compressive stresses and undeformed/deformed configurations. This work used a new FE model (presented in Chapter 3), and goes on to describes the detailed process leading to the optimized design.

4.3. Methods

4.3.1. Finite Element Model

The FE modelling was implemented using a parametric code developed in a commercially available FE package (ANSYS®). This model was a planar model with the assumption of plane stress. Material nonlinearities of skin were modeled using a two-term Ogden hyperelastic model

(Ogden, 1997, 1972), where strain energy density W_0 was defined as a function of the principal stretches λ_1, λ_2, and λ_3 such that

$$W_0 = \sum_{p=1}^{2} \frac{\mu_p}{\alpha_p} \left(\lambda_1^{\alpha_p} + \lambda_2^{\alpha_p} + \lambda_3^{\alpha_p} - 3 \right), \tag{4.1}$$

where the coefficients μ_p and α_p are material constants. Due to the short time required for wound closure, time-dependent properties were neglected (Jor et al., 2011; Kirby et al., 1998; Lapeer et al., 2010; Ní Annaidh et al., 2012). An assumption of isotropy was applied to facilitate simple comparisons between different flaps, focusing on the material and geometric nonlinearities and avoiding extra directional variables (the correct choice of the flap orientation, with respect to the skin's line of maximum extensibility (LME) and the relaxed skin tension line (RSTL), will be made by investigating the boundary forces). By adapting a range of data from Ní Annaidh et al. (2012), four sets of material constants were considered (Table 4.1), and the corresponding stress-stretch plots are shown in Figure 4.1.

Table 4.1 Four different sets of material constants for the Ogden hyperelastic model

	μ_1 (MPa)	α_1	μ_2 (MPa)	α_2
Material 1	0.0289	22.2	-1.49	-1.00
Material 2	0.0369	17.3	-1.03	-2.00
Material 3	0.0494	12.5	-0.580	-3.00
Material 4	0.0720	9.37	-0.325	-4.00

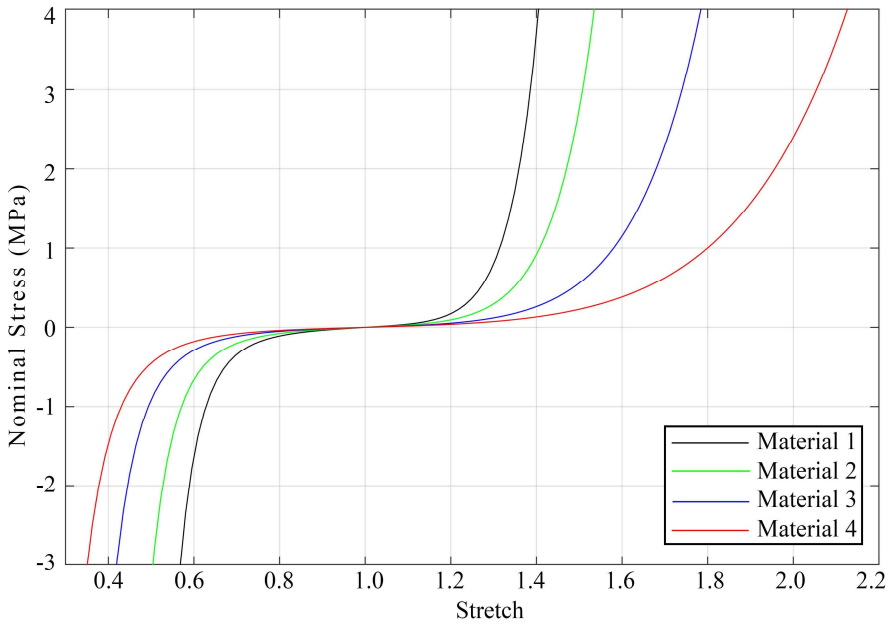

Figure 4.1 The plot of nominal stress vs. stretch for the material models used in this research, assuming plane stress and uniaxial loading

The parametric configuration of the rhombic flap is shown in Figure 4.2(a), with all sides being equal; ϕ is the acute angle of the rhombic defect ABCD; θ_1 is an angle between the line extended from the short diagonal BD and the first incision DE; and θ_2 is the angle measured from the first incision DE to the second incision EF. Given this parametric configuration, the Limberg flap can be constructed by $\phi = \theta_2 = 60°$, $\theta_1 = 0$, and the Dufourmentel can be constructed for any ϕ between 60° and 90° with $\theta_1 = 45° - \phi/4$ and $\theta_2 = 45° + \phi/4$. In this study, all the sides were considered to have the same length of 30 mm. Skin thickness was considered to be uniform with a value of 1.50 mm, based on average amounts reported in the literature (Groves et al., 2013; Reihsner et al., 1995). Figure 4.2(b) also shows part of the discretized geometry developed using ANSYS®. To avoid the issue of stress singularity (Danielson, 1978), sharp corners at critical regions (which prevent stress convergence) were replaced with round corners. There exists a fixed outer circular boundary with a diameter of 300 mm, and a small gap of 0.60 mm at the incisions DE and EF. For the purpose of the comparative study, a total number of 8,000 elements was found to be appropriate

such that differences between the models converged. The values for the gap width and the number of elements was made through a trial and error process aiming to obtain a balance between accuracy and computational expense. The choice of the outer circular boundary was also made so that, for each simulation, changing the length of each side by 30% had negligible effects on stress and deformation results.

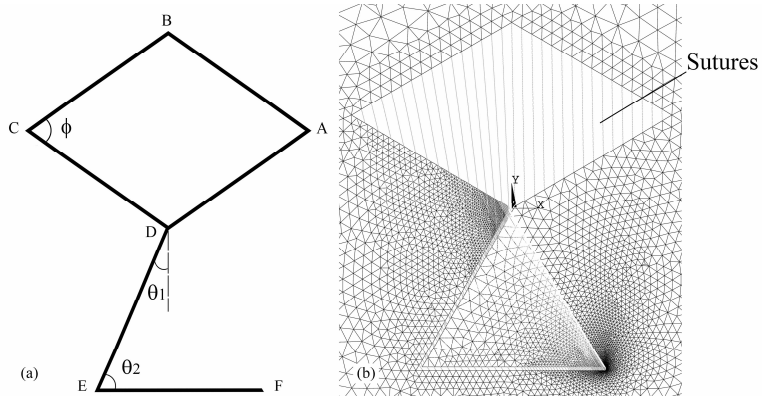

Figure 4.2 (a) The parametric configuration to be optimized (b) part of the geometric model and meshing (this part is surrounded by a circular boundary which is not shown here)

To simulate the process of wound closure by sutures, a number of similar elements were connected to the nodes along the wound that are expected to be placed beside each other in the final deformed configuration. By applying the same artificial temperature change and defining the same thermal contraction coefficient to all the connector elements, the process of wound closure was simulated. The product of cross sectional area and elastic modulus of the elements was deemed sufficiently large to ensure that the shrinkage of the elements is not stopped by any opposing force exerted by the tissue. To achieve a simulation which was accurate, yet reasonable in terms of computational expense, an engineering strain of -3.3 was applied to all the connecting elements.

4.3.2. Virtual Experiment Design

To obtain an optimized version for rhombic flaps, a number of simulations were performed using different configurations and material models. Based on the general operational trends towards sixty-degree rhombic defects, the initial simulations were performed considering $\phi = 60°$. In this case, 9 values for the angle θ_1 (range: -10° to 70°, 10° increments) and 6 values for the angle θ_2 (range: 30° to 80°, 10° increments) were considered using the 4 different skin models. This yielded 216 virtual experiments. FE outcomes included: maximum von Mises stress, maximum tensile principal stress, maximum compressive principal stress, and the deformed configuration for each single simulation. To specify optimized configurations, the values for means and standard deviations were examined, and deformation considerations were applied. Based on the optimal pattern determined for the case of $\phi = 60°$, similar configurations were investigated for $\phi = 70°$, 80°, and 90° to ensure the generalization for all the defect angles between 60° and 90°. For all simulations, the stress values were expressed in terms of normalized amounts to facilitate a proper comparative study. An equal value of thermal contraction (logarithmic strain of -3.3) was applied to all the connecting elements in all the configurations.

4.4. Results

Figure 4.3 and Figure 4.4 show the plot of normalized maximum von Mises stress and normalized maximum compressive principal stress, respectively, for $\phi = 60°$. The maximum tensile principal stresses was not included as it was almost identical to the von Mises stress plot. To provide insight into the deformation outcomes, moreover, a number of deformed configurations illustrating the suture lines are shown in Figure 4.5. Low dependency on material constants was observed for the deformations.

Considering von Mises, tensile, and compressive stresses as well as deformation results, the flap featuring $\theta_1 = \theta_2 = 60°$ appeared to be the optimized version of rhombic transposition flap for $\phi = 60°$. Based on our simulations using 4 material models, the proposed flap offered 43% lower max von Mises stress relative to the classical Limberg flap. As a comparison, the Dufourmentel flap resulted in 27% lower stress relative to the Limberg flap. The maximum compressive stress in the proposed method was also found to be within the limits of those occurring in the flaps of Limberg and Dufourmentel. Figure 4.6 shows the distribution of von Mises stress in the proposed flap as compared to the corresponding distributions in the flaps of Limberg and Dufourmentel. The general patterns remain almost the same for different material models.

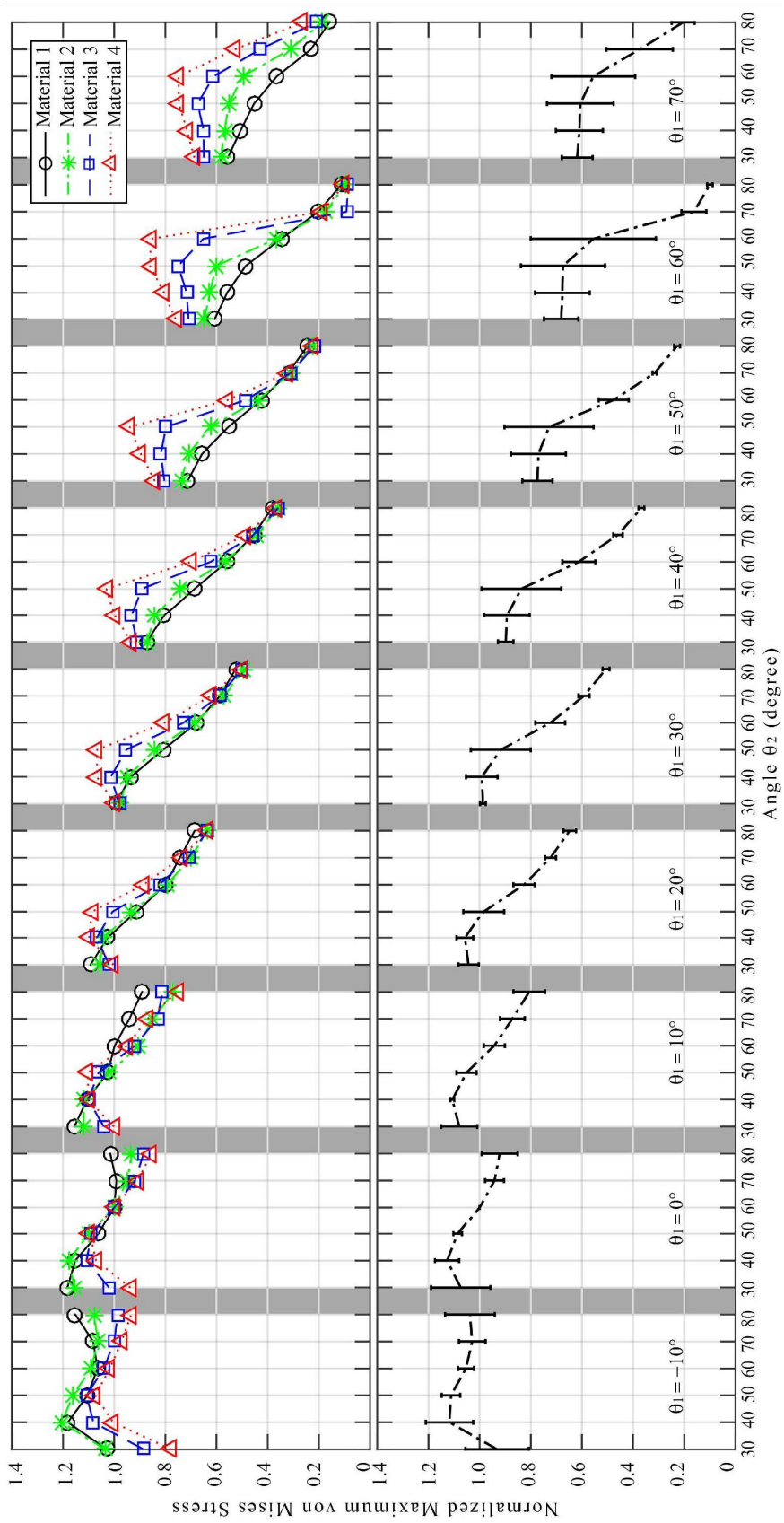

Figure 4.3 The maximum von Mises stress vs. the angles θ_1 and θ_2 for $\phi = 60°$. For each material, the stress values were normalized with respect to the stress value of the Limberg flap modeled using that material model. The mean and standard deviation values are shown in the bottom plot.

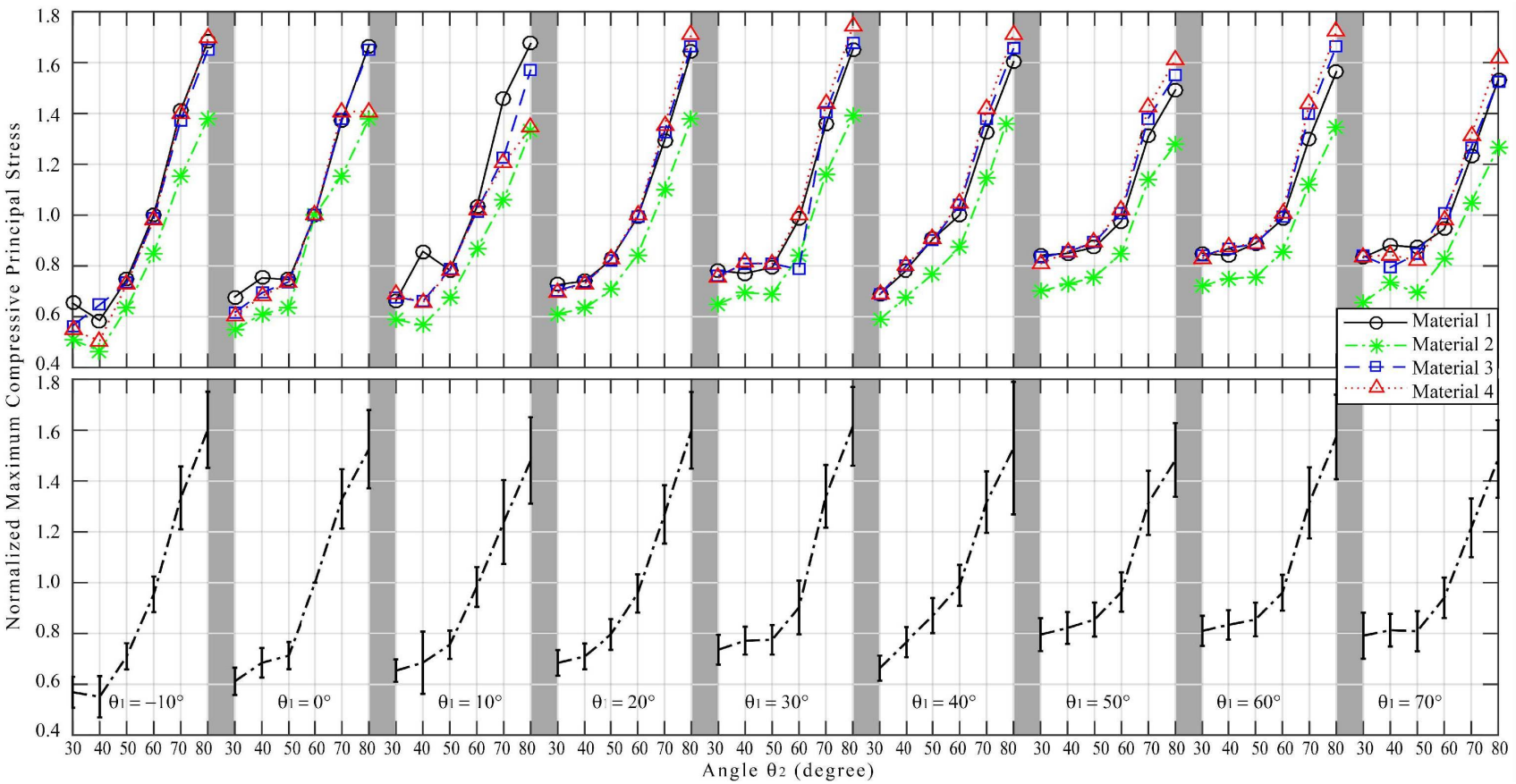

Figure 4.4 The maximum compressive principal stress vs. the angles θ_1 and θ_2 for $\phi = 60°$. For each material, the stress values were normalized with respect to the stress value of the Limberg flap modeled using that material model. The mean and standard deviation values are shown in the bottom plot.

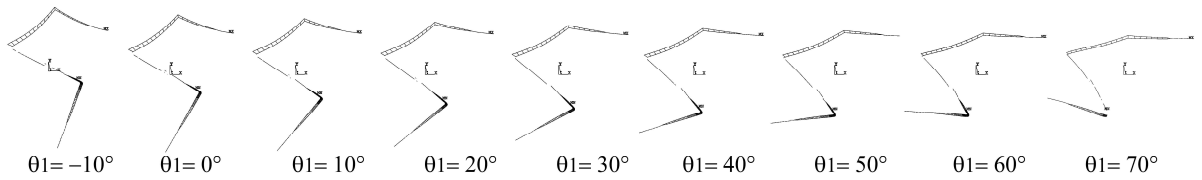

Figure 4.5 Deformed configurations showing the suture lines. All the cases pertain to material 1 with $\phi = \theta_2 = 60°$.

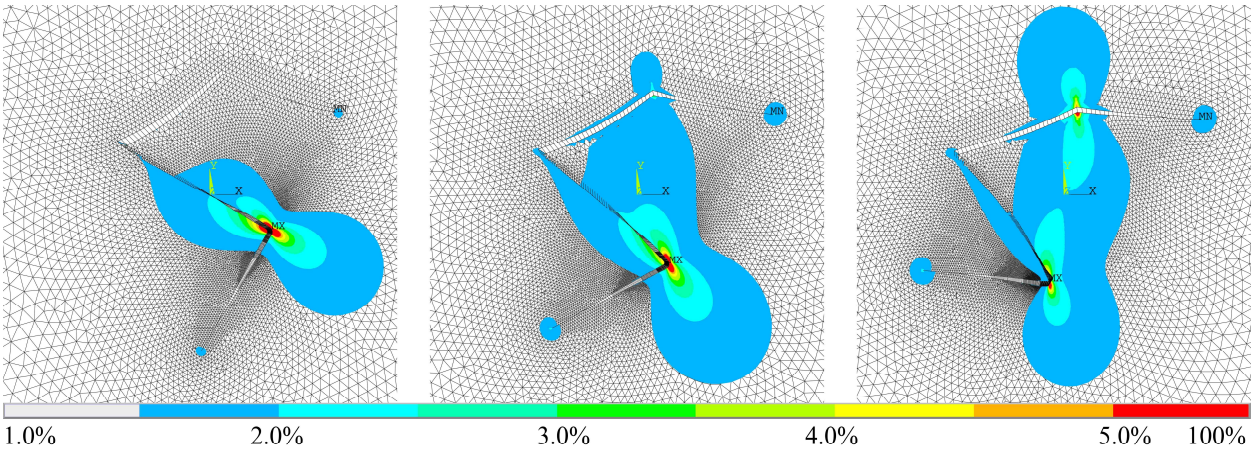

Figure 4.6 Contour plot of von Mises stress in the Limberg flap (left), the Dufourmentel flap (middle), and the proposed flap (right). For all three configurations, $\phi = 60°$, with material 3.

To generalize the proposed flap to other values of ϕ, the first incision DE was considered to be co-linear with defect side AD, and the flap angle θ_2 was considered to be the same as the angle ϕ (Figure 4.7). The results of force analysis at the outer circular boundary suggests that, with surgery, placing the flap base DF along LME leads to the most efficient outcomes for the proposed configuration (this is consistent with the procedures outlined by Lister and Gibson (1972) and Cuono (1983)). Figure 4.8 shows the plots of normalized von Mises stress with respect to ϕ for the proposed flap. On average, when compared to the Dufourmentel flap, the proposed flap can reduce the maximum von Mises stress by 53%

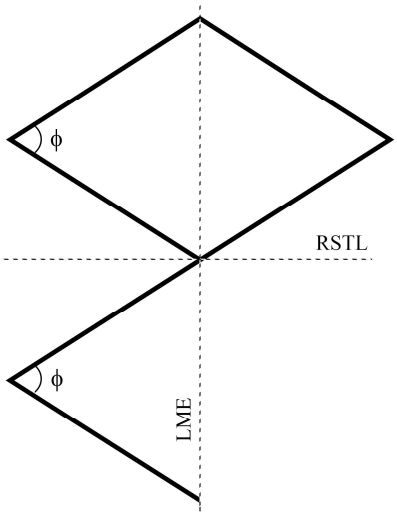

Figure 4.7 The proposed flap. All the sides are equal to each other and the angle ϕ can have any value between 60° and 90°. The orientation with respect to LME and RSTL is also shown.

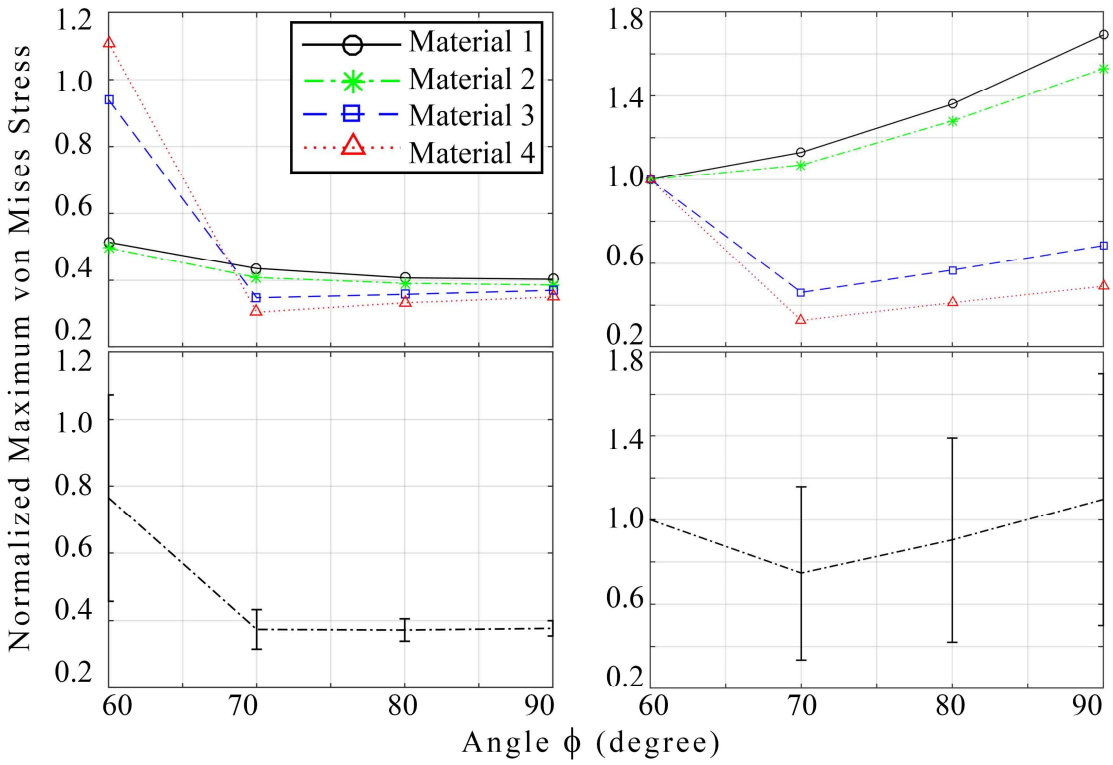

Figure 4.8 Plot of the maximum von Mises stress for the proposed flap: (left) for each material and each specific configuration, the stress values are normalized with respect to the corresponding values in the Dufourmentel flap; (right) for each material, the stress values are normalized with respect to their initial values at $\phi = 60°$.

4.5. Discussion

Among all the simulated configurations, the proposed optimal flap was selected based on the maximum von Mises and tensile stresses, considering constraints on compressive stresses and deformations. In the proposed flap, the maximum values for both von Mises and the principal tensile stresses were reduced by partial elimination of stress concentrations. This was evident from our results. Stress distributed in the proposed flap in a bipolar manner, while with other flaps, the stress fields were more of a unipolar pattern leading to large stress concentrations. The amount of compressive stress in the proposed flap was also compared to the flaps of Limberg and Dufourmentel. Of note, such compressive stresses do not occur in reality (Danielson and Natarajan, 1975) and they are an indicator suggesting depressed areas such as the formation of dog-ears. Therefore, low compressive stresses, as seen in the proposed flap, are preferable.

Our results also showed a considerable stress improvement in the proposed configuration with respect to the Dufourmentel flap, where, for the majority of configurations, the maximum stress was reduced by more than 60%. However, it should be noted that these results do not imply which configuration is best; they only demonstrate stress enhancement compared to each corresponding configuration of the Dufourmentel flap. Our analyses of different ϕ showed that there is not a single angle ϕ which is best for all materials. This issue appears to be caused from considerable dependency on the material models, as implied by variance (i.e. standard deviations). Although our results suggest that a 70° defect can produce an optimal pattern (on average), the choice of ϕ should be made by taking into account tissue availability and case-specific considerations (e.g. stiff versus flexible skin).

In addition to the aforementioned stress characteristics, ease of construction was another important feature offered by the proposed flap. After a rhombic defect with any angle ϕ is selected

by the surgeon, the incisions can be easily made using similar angles with the defect. In addition to ease of construction, the placement of the flap with respect to direction of the LME and RSTL was facilitated. Since the flap base DF and the short diagonal BD lie along each other, the favorable flap orientation can be achieved by adjusting the short diagonal along the LME. This corresponds to placing the long diagonal AC along RSTL.

Multiple regression identified another interesting observation pertaining to maximum compressive stresses, specifically that they varied varying mostly with respect to θ_2 ($p < 0.0001$), while almost no considerable change was noticed with respect to θ_1 ($p = 0.095$). This implies a weak link between the maximum compressive stress and θ_1 and a strong link with θ_2. This can account for the fact that there was almost no difference in compressive stress occurring in the Limberg flap, Dufourmentel flap, and the proposed flap for a 60° defect angle. For other values of ϕ, the maximum compressive stress in the proposed flap was found to be only 8% (on average) more than that occurring in the Dufourmentel flap.

By a careful examination of the proposed flap, it is interesting to note that the constructed triangular tissues CDE and DEF, as well as the way they are transposed to facilitate wound closure, are analogous to those associated with Z-plasty surgery (Hove et al., 2001; Hudson, 2000) with a flap angle of ϕ. In this way, the classic 60° Z-plasty is similar to the 60° rhombic flap with the proposed configuration. From this perspective, the proposed flap can be deemed as a fusion of the rhombic transposition flap and Z-plasty, two common techniques widely used in plastic surgery. The proposed flap in this study is comparable in concept to an earlier flap design proposed by Becker (1979). This method (that is introduced by Becker as a “rhomboid-to-W” technique) incorporates W-plasty into the rhomboid defects and has had many applications in plastic surgery

(Cuono, 1983; Gahhos and Cuono, 1990; Harashina and Kubota, 1982; Izaguirre and Navarro, 1983; Keser et al., 1998; Wheeland, 1991).

Regarding limitations, this study was conducted by taking into consideration a number of assumptions, particularly skin modelling. Although different material constants were examined, all of them were defined using the Ogden material model (Ogden, 1972). It is suggested that, in similar comparative studies, different material models be considered, such as the hyperelastic models proposed by Yeoh (1990), Arruda and Boyce (1993), and Gent (1996). It should be also noted that although our assumption of isotropy, here, created a great deal of simplification and ease for the purpose of comparisons, such an assumption, in general, cannot account for the exact behavior of a particular type of skin in a specific problem. Skin also shows time-dependent characteristics such as creep and stress relaxation. Whereas such properties, by alleviation of undesirable effects of intense stresses, can save a poorly designed/implemented flap, it is not recommended to consider them as a design parameter (Larrabee and Bloom, 2007). To avoid such a large geometric variability, topological features were dismissed and a planar model with plane stress was considered. A three-dimensional model would be required for the study of out-of-plane deformations (such as formation of wrinkles or dog-ears) and case-specific problems.

5. Conclusions

This research was conducted by considering two main objectives:

1) development of a reliable FE code to serve as a framework for virtual experiments; and
2) design of an optimized rhombic transposition flap by focusing on minimization of maximum von Mises stress and taking into consideration constraints on maximum compressive stress and undeformed/deformed configurations.

The first objective was the outlined in the Chapter 3, where a reliable FE framework was developed and its performance in predicting stress/deformation results was observed to be consistent with real surgery. Using this FE tool, the second objective (which was the general objective of this research) was addressed in Chapter 4, where a rhombic transposition flap was designed. The proposed flap considerably reduced the maximum von Mises stress while maintaining the maximum compressive stress and deformed configuration within reasonable limits.

The main contributions of this study include:

1) devising a simple method to simulate the process of wound closure by means of two-force elements and thermal contraction property;
2) solving the issue of stress singularity to ensure convergence in FE simulations of rhombic flaps;
3) employing different material models for skin in the comparative study; and
4) designing an optimized rhombic flap.

Based on the results and analysis in this thesis, recommendations for future research include:

1) Practical experiments are required before the proposed flap should be used in real surgeries. This task may be initiated by experiments on rubber-like materials which behave in a similar fashion to human skin. After initial assessment, a number of practical tests should be performed on animal/human subjects.
2) The approach presented in this research can be utilized not only to optimize other techniques currently used for wound closure, but to create conceptually new techniques in plastic surgery.
3) Finally, it is also suggested that, in future studies, different constitutive models be considered together with different sets of constants for each model.

References

Arruda, E.M., Boyce, M.C., 1993. A three-dimensional constitutive model for the large stretch behavior of rubber elastic materials. J. Mech. Phys. Solids 41, 389–412.

Becker, H., 1979. The rhomboid-to-W technique for excision of some skin lesions and closure. Plast. Reconstr. Surg. 64, 444–7.

Berardesca, E., de Rigal, J., Leveque, J.L., Maibach, H.I., 1991. In vivo biophysical characterization of skin physiological differences in races. Dermatologica 182, 89–93.

Borges, A.F., 1978. Choosing the correct Limberg flap. Plast. Reconstr. Surg. 62, 542–5.

Borges, A.F., 1984. Relaxed skin tension lines (RSTL) versus other skin lines. Plast. Reconstr. Surg. 73, 144–50.

Brown, I.A., 1972. Scanning electron microscopy of human dermal fibrous tissue. J. Anat. 113, 159–68.

Bucalo, B.D., Iriondo, M., 1995. Photoelastic Models of Wound Closure Stress. Dermatologic Surg. 21, 210–212.

Buganza-Tepole, A., Steinberg, J.P., Kuhl, E., Gosain, A.K., 2014. Application of finite element modeling to optimize flap design with tissue expansion. Plast. Reconstr. Surg. 134, 785–92.

Cacou, C., Muir, I.F., 1995. Effects of plane mechanical forces in wound healing in humans. J. R. Coll. Surg. Edinb. 40, 38–41.

Capaldi, F.M., 2012. Continuum Mechanics: Constitutive Modeling of Structural and Biological Materials. Cambridge University Press.

Capek, L., Dzan, L., Ackermann, M., 2011. Three-dimensional finite element analysis of rhomboid flap. Int. J. Oral Maxillofac. Surg. 40, 1121.

Chaudhry, H.R., Bukiet, B., Siegel, M., Findley, T., Ritter, A.B., Guzelsu, N., 1998. Optimal patterns for suturing wounds. J. Biomech. 31, 653–62.

Cuono, C.B., 1983. Double Z-plasty repair of large and small rhombic defects: the double-Z rhomboid. Plast. Reconstr. Surg.

Daly, C.H., 1982. Biomechanical properties of dermis. J. Invest. Dermatol. 79 Suppl 1, 17s–20s.

Daly, C.H., Odland, G.F., 1979. Age-related changes in the mechanical properties of human skin. J. Invest. Dermatol. 73, 84–7.

Danielson, D.A., 1978. Tension field theories for soft tissues. Bull. Math. Biol. 40, 161–182.

Danielson, D.A., Natarajan, S., 1975. Tension field theory and the stress in stretched skin. J. Biomech. 8, 135–142.

Dufourmentel, C., 1962. Le fermeture des pertes de substance cutanée limitées “Le lambeau de rotation en L pour losange” dit “LLL.” Ann. Chir. Plast. 7, 61–66.

Escoffier, C., de Rigal, J., Rochefort, A., Vasselet, R., Lévêque, J.L., Agache, P.G., 1989. Age-related mechanical properties of human skin: an in vivo study. J. Invest. Dermatol. 93, 353–7.

Faller, A., Schünke, M., Schünke, G., Taub, E., 2004. The Human Body: An Introduction to Structure and Function. Thieme.

Flynn, C., 2010. Finite element models of wound closure. J. Tissue Viability 19, 137–49.

Furr, M.C., Wang, T.D., 2011. Complex local flap design in cheek reconstruction. Oper. Tech. Otolaryngol. - Head Neck Surg. 22, 53–58.

Gahhos, F.N., Cuono, C.B., 1990. Double-Z rhombic technique for reconstruction of facial wounds. Plast. Reconstr. Surg.

Gennisson, J.-L., Baldeweck, T., Tanter, M., Catheline, S., Fink, M., Sandrin, L., Cornillon, C., Querleux, B., 2004. Assessment of elastic parameters of human skin using dynamic elastography. IEEE Trans. Ultrason. Ferroelectr. Freq. Control 51, 980–989.

Gent, A.N., 1996. A new constitutive relation for rubber. Rubber Chem. Technol. 69, 59–61.

Gladwell, G.M.L., 1980. Contact Problems in the Classical Theory of Elasticity. Springer Science & Business Media.

Grahame, R., 1970. A method for measuring human skin elasticity in vivo with observations of the effects of age, sex and pregnancy. Clin. Sci. 39, 223–9.

Groves, R.B., Coulman, S.A., Birchall, J.C., Evans, S.L., 2013. An anisotropic, hyperelastic model for skin: experimental measurements, finite element modelling and identification of parameters for human and murine skin. J. Mech. Behav. Biomed. Mater. 18, 167–80.

Harashina, T., Kubota, J., 1982. Further applications of the rhomboid-to-W technique. Ann. Plast. Surg. 9, 211–5.

Hove, C.R., Williams, E.F., Rodgers, B.J., 2001. Z-plasty: a concise review. Facial Plast. Surg. 17, 289–94.

Hudson, D. a, 2000. Some thoughts on choosing a Z-plasty: the Z made simple. Plast. Reconstr. Surg. 106, 665–671.

Izaguirre, H., Navarro, C., 1983. Rhomboid-to-“W” technique for excision and closure of facial skin lesions. J. Maxillofac. Surg. 11, 207–210.

Jong, L.A.M. de, 1995. Pre-tension and anisotropy in skin : modelling and experiments. Eindhoven University of Technology.

Jor, J.W.Y., Nielsen, P.M.F., Nash, M.P., Hunter, P.J., 2011. Modelling collagen fibre orientation in porcine skin based upon confocal laser scanning microscopy. Ski. Res. Technol. 17, 149–159.

Kawabata, H., Kawai, H., Masada, K., Ono, K., 1989. Computer-Aided Analysis of Z-Plasties. Plast. Reconstr. Surg. 83, 319–325.

Keser, A., Sensöz, O., Mengi, A.S., 1998. Double opposing semicircular flap: a modification of opposing Z-plasty for closing circular defects. Plast. Reconstr. Surg. 102, 1001–7.

Kirby, S.D., Wang, B., To, C.W., Lampe, H.B., 1998. Nonlinear, three-dimensional finite-element model of skin biomechanics. J. Otolaryngol. 27, 153–160.

Langer, K., 1978. On the anatomy and physiology of the skin. Br. J. Plast. Surg. 31, 3–8.

Lapeer, R.J., Gasson, P.D., Karri, V., 2010. Simulating plastic surgery: From human skin tensile tests, through hyperelastic finite element models to real-time haptics. Prog. Biophys. Mol. Biol. 103, 208–216.

Larrabee, W.F., 1986. A finite element model of skin deformation. I. Biomechanics of skin and soft tissue: a review. Laryngoscope 96, 399–405.

Larrabee, W.F., Bloom, D.C., 2007. Local Flaps in Facial Reconstruction. In: Baker, S.R. (Ed.), Local Flaps in Facial Reconstruction. Elsevier Health Sciences, pp. 31–40.

Larrabee, W.F., Galt, J.A., 1986. A finite element model of skin deformation. III. The finite element model. Laryngoscope 96, 413–419.

Limberg, A.A., 1946. Mathematical principles of local plastic procedures on the surface of the human body. Medgis.

Limberg, A.A., 1966. Modern trends in plastic surgery. Design of local flaps. Mod. Trends Plast. Surg. 2, 38–61.

Lister, G.D., Gibson, T., 1972. Closure of rhomboid skin defects: The flaps of Limberg and Dufourmentel. Br. J. Plast. Surg. 25, 300–314.

Lott-Crumpler, D. a, Chaudhry, H.R., 2001. Optimal patterns for suturing wounds of complex shapes to foster healing. J. Biomech. 34, 51–58.

Manios, A., Katsantonis, J., Tosca, A., Skulakis, C., Tsiftsis, D., 1996. The Finite Element Method as a Research and Teaching Tool in the Analysis of Local Skin Flaps. Dermatologic Surg. 22, 1029–1033.

Mathew, J., Varghese, S., Jagadeesh, S., 2008. The Limberg flap for cutaneous defects — a two year experience. Indian J. Surg. 69, 184–186.

McNay, A.T., Ostad, A., Moy, R.L., 1997. Surgical Pearl: Modified rhombic flap. J. Am. Acad. Dermatol. 37, 256–258.

Ní Annaidh, A., Bruyère, K., Destrade, M., Gilchrist, M.D., Otténio, M., 2012. Characterization of the anisotropic mechanical properties of excised human skin. J. Mech. Behav. Biomed. Mater. 5, 139–48.

O'Brien, J., Wysocki, J., Anastasi, G., 1976. Limberg flap coverage for axillary defects resulting from excision of hidradenitis suppurativa. Plast. Reconstr. Surg. 58, 354–8.

Ogden, R.W., 1972. Large Deformation Isotropic Elasticity - On the Correlation of Theory and Experiment for Incompressible Rubberlike Solids. Proc. R. Soc. A Math. Phys. Eng. Sci. 326, 565–584.

Ogden, R.W., 1997. Non-linear Elastic Deformations. Courier Corporation.

Patel, K.G., Sykes, J.M., 2011. Concepts in local flap design and classification. Oper. Tech. Otolaryngol. - Head Neck Surg. 22, 13–23.

Pauchot, J., Remache, D., Chambert, J., Elkhyat, A., Jacquet, E., 2012. Finite element analysis to determine stress fields at the apex of V-Y flaps. Eur. J. Plast. Surg. 36, 185–190.

Pieper, S.D., Laub, D.R., Rosen, J.M., 1995. A finite-element facial model for simulating plastic surgery. Plast. Reconstr. Surg. 96, 1100–5.

Quaba, A.A., Sommerlad, B.C., 1987. "A square peg into a round hole": a modified rhomboid flap and its clinical application. Br. J. Plast. Surg. 40, 163–170.

Reihsner, R., Balogh, B., Menzel, E.J., 1995. Two-dimensional elastic properties of human skin in terms of an incremental model at the in vivo configuration. Med. Eng. Phys. 17, 304–313.

Reihsner, R., Menzel, E.J., 1998. Two-dimensional stress-relaxation behavior of human skin as influenced by non-enzymatic glycation and the inhibitory agent aminoguanidine. J. Biomech. 31, 985–993.

Seidenari, S., Pagnoni, A., Di Nardo, A., Giannetti, A., 1994. Echographic evaluation with image analysis of normal skin: variations according to age and sex. Skin Pharmacol. 7, 201–9.

Sifakis, E., Hellrung, J., Teran, J., Oliker, A., Cutting, C., 2009. Local flaps: a real-time finite element based solution to the plastic surgery defect puzzle. Stud. Health Technol. Inform. 142, 313–8.

Topp, S.G., Lovald, S., Khraishi, T., Gaball, C.W., 2014. Biomechanics of the Rhombic Transposition Flap. Otolaryngol. -- Head Neck Surg. 151, 952–959.

Uraiqat, A., 2010. Dufourmentel Flap for the Treatment of Pilonidal Sinus Disease. J. R. Med. Serv. 17, 35–40.

Wheeland, R.G., 1991. Reconstruction of the lower lip and chin using local and random-pattern flaps. J. Dermatol. Surg. Oncol. 17, 605–15.

Wilkes, G.L., Brown, I.A., Wildnauer, R.H., 1973. The biomechanical properties of skin. CRC Crit. Rev. Bioeng. 1, 453–95.

Wilson, D., Berardesca, E., Maibach, H.I., 1988. In vitro transepidermal water loss: differences between black and white human skin. Br. J. Dermatol. 119, 647–52.

Yeoh, O.H., 1990. Characterization of Elastic Properties of Carbon-Black-Filled Rubber Vulcanizates. Rubber Chem. Technol. 63, 792–805.

Yoshida, H., Tsutsumi, S., Mizunuma, M., Yanai, A., 2000. Three-dimensional finite element analysis of skin suture. Med. Eng. Phys. 22, 481–485.